PHYSICAL REVIEW D **83,** 123001 (2011)

Improvement of low energy atmospheric neutrino flux calculation using the JAM nuclear interaction model

M. Honda*
Institute for Cosmic Ray Research, the University of Tokyo, 5-1-5 Kashiwa-no-ha, Kashiwa, Chiba 277-8582, Japan

T. Kajita†
Institute for Cosmic Ray Research, and Institute for the Physics and Mathematical of the Universe, the University of Tokyo, 5-1-5 Kashiwa-no-ha, Kashiwa, Chiba 277-8582, Japan

K. Kasahara‡
Research Institute for Science and Engineering, Waseda University, 3-4-1 Okubo Shinjuku-ku, Tokyo, 169-8555, Japan

S. Midorikawa§
Faculty of Software and Information Technology, Aomori University, Aomori, 030-0943 Japan
(Received 18 February 2011; published 2 June 2011)

We present the calculation of the atmospheric neutrino fluxes with an interaction model named JAM, which is used in PHITS (Particle and Heavy-Ion Transport code System) [K. Niita *et al.*, Radiation Measurements **41**, 1080 (2006).]. The JAM interaction model agrees with the HARP experiment [H. Collaboration, Astropart. Phys. **30**, 124 (2008).] a little better than DPMJET-III [S. Roesler, R. Engel, and J. Ranft, arXiv:hep-ph/0012252.]. After some modifications, it reproduces the muon flux below 1 GeV/c at balloon altitudes better than the modified DPMJET-III, which we used for the calculation of atmospheric neutrino flux in previous works [T. Sanuki, M. Honda, T. Kajita, K. Kasahara, and S. Midorikawa, Phys. Rev. D **75**, 043005 (2007).][M. Honda, T. Kajita, K. Kasahara, S. Midorikawa, and T. Sanuki, Phys. Rev. D **75**, 043006 (2007).]. Some improvements in the calculation of atmospheric neutrino flux are also reported.

DOI: 10.1103/PhysRevD.83.123001 PACS numbers: 95.85.Ry, 13.85.Tp, 14.60.Pq

I. INTRODUCTION

We have calculated atmospheric neutrino fluxes using a 3D scheme, and refined it in previous works [1,2]. In Ref. [3], we studied reputable interaction models with the atmospheric muon spectrum at balloon altitudes, and selected DPMJET-III [3]. We then constructed and used an inclusive interaction code, which has virtually the same secondary production spectra as DPMJET-III, but which runs far more rapidly (see Appendix A). However, when we compare the high energy muon flux calculated using DPMJET-III with the observed fluxes at sea level and mountain altitudes, there are obvious deficiencies in the calculated values at high momenta ($\gtrsim 30$ GeV/c) [4]. Therefore, we modified the ''inclusive DPMJET-III'' so that the calculation reproduces the observed atmospheric muon spectra with better accuracy at high momenta, and used it in the calculation of the atmospheric neutrino fluxes [1]. We called the modified inclusive interaction code the ''modified DPMJET-III.'' Below 5 GeV, we used the inclusive NUCRIN which is constructed from NUCRIN [5] with some modifications. However, the contributions of the hadronic interaction below 5 GeV to the atmospheric neutrino and muon fluxes even at around 1 GeV/c and below are smaller than those above 5 GeV.

With the ''modified DPMJET-III,'' we could reproduce the observed atmospheric muon spectra quite well above 1 GeV/c at sea level and mountain altitudes, but the agreement below 1 GeV/c is not as good. At balloon altitudes, in particular, the calculated muon fluxes are obviously lower than the observed ones. This seems to be due to the secondary spectra of DPMJET-III, which our simple modification procedure (see Appendix A) cannot correct. The disagreement was not resolved without violating the agreement at higher momenta. Instead of a more sophisticated modification method, we searched for an interaction model which has a better nature at low energies, and found the interaction model called JAM, which is used in PHITS (Particle and Heavy-Ion Transport code System) [6]. JAM is useful from much lower projectile energies ($\ll 0.1$ GeV) up to $\sim$100 GeV.

Apart from the atmospheric muon flux, the HARP experiment has greatly improved our knowledge of the hadronic interaction at low energies [7]. It is notable that the hadronic interactions of protons on thin N_2 and O_2 targets have been studied in detail by the HARP experiment, aiming to improve the calculation of atmospheric neutrino fluxes [8]. They found that the commonly used hadronic interaction models including DPMJET-III do not reproduce the result of the HARP experiment accurately, especially

*mhonda@icrr.u-tokyo.ac.jp; http://icrr.u-tokyo.ac.jp/~mhonda
†kajita@icrr.u-tokyo.ac.jp
‡kasahara@icrc.u-tokyo.ac.jp
§midori@aomori-u.ac.jp

for the π^- productions [7]. We examine JAM also with the HARP data, and find the JAM agrees a little better than DPMJET-III.

Then, we construct the inclusive interaction code for JAM and studied the atmospheric muon flux with it at sea level, at mountain altitudes, and at balloon altitudes. The ''inclusive JAM'' is used for hadronic interactions from 0.2 GeV to 32 GeV, and above these energies, the modified DPMJET-III is used as before. After some modifications for the inclusive JAM, we can reproduce the observed atmospheric muon flux below 1 GeV/c at sea level and at balloon altitudes, but the agreement of the atmospheric muon flux at the mountain altitudes becomes worse. As we can carry out a study similar to the previous publication [4] between the muons at balloon altitudes and the interaction model relevant to the low energy ($\lesssim$ 1 GeV) atmospheric neutrinos, we consider the agreement at balloon altitudes to be more important, and use it for the calculation of the atmospheric neutrino fluxes.

The calculation scheme is essentially the same as that used in Ref. [2], although we are refining it in each work. In this work, we optimized the ''virtual detector correction'' to minimize the statistical errors. Also with the increase of the available computation power, we calculate the atmospheric neutrino fluxes in this 3D scheme up to 32 GeV. We find that the calculated atmospheric neutrino fluxes show a visible azimuthal dependence below 32 GeV.

The change of interaction model and refinement of the calculation scheme notwithstanding, the zenith angle dependence of the atmospheric neutrino fluxes and the $(\nu_\mu + \bar{\nu}_\mu)/(\nu_e + \bar{\nu}_e)$ ratio are very close to the previous calculations. The change of the hadronic interaction model mainly results in a change to the absolute value of the atmospheric neutrino flux below 1 GeV.

II. INTERACTION MODEL AND CALCULATION OF ATMOSPHERIC NEUTRINO FLUX

The requirements for the hadronic interaction model used in the calculation of atmospheric neutrino fluxes are that it reproduces the real hadronic interaction accurately, and that the code generates hadronic events very quickly. The first requirement is a general requirement for all applications of the hadronic interaction model.

We collected the reputable interaction models, and examined them with available accelerator data. We further examined them with the atmospheric muon flux observed at balloon altitudes. As a result, we selected DPMJET-III for our calculations in Ref. [2]. Note, DPMJET-III is not usable below $\sim$5 GeV in projectile energy, and so we used NUCRIN below 5 GeV.

The second requirement often conflicts with the first one. The computer code of a sophisticated interaction model generally takes a lot of time to generate an interaction event. To resolve this conflict, we construct a quick inclusive interaction code, which generates virtually the same secondary production spectra as the original interaction model from the output of the original code. We explain the construction of the inclusive code in some detail in Appendix A. The interaction code used in Ref. [2] was such an inclusive code, made from the output of original code of DPMJET-III, and was called the inclusive DPMJET-III. The inclusive code is useful for the calculation of the time averaged quantity, but is not usable for the simulation of an event caused by a high energy cosmic ray, such as an air shower.

The use of the inclusive code has the advantage that we can simply modify the secondary spectra of the original interaction model without detailed knowledge of the assumptions internal to it. We modified the inclusive DPMJET-III in the procedure explained in Appendix A, and we could reproduce the observed atmospheric muon flux above 1 GeV with satisfactory accuracy at sea-level and mountain altitude [4]. The modification changes the gradient of secondary spectra globally, and is effectively a change of the so called Z-factor ($Z \equiv \langle x^{1.7} \rangle$ with $x \equiv E_{\rm secondary}/E_{\rm projectile}$), which describes the atmospheric muon and neutrino fluxes at high energies well [9]. The power of 1.7 is approximately the spectral index of the integral cosmic ray nucleon flux. We called it modified DPMJET-III, and calculated the atmospheric neutrino flux with it [1].

With the modification, however, we could not reproduce the observed atmospheric muon flux below $\sim$1 GeV/c. The cosmic ray energies relevant to the atmospheric muon at 1 GeV/c are around 10 GeV or lower, depending on the observing altitude, and the cosmic ray spectrum can no longer be approximated by a single power law there. The structure of the secondary spectra, which does not have much influence on the Z-factor, becomes important. The disagreement between calculations and observations in the low energy atmospheric muon is due to such a structure in the DPMJET-III model at low projectile energies ($\lesssim$ 10 GeV). One approach to improving the agreement would be developing a more sophisticated and complicated modification procedure. However, we have taken an alternative approach and looked for an interaction model which has a better low energy behavior than DPMJET-III, and have found an interaction model called JAM which is used in the PHITS (Particle and Heavy-Ion Transport code System) [6].

After our previous calculation, the HARP collaboration released a much more detailed study of hadronic interactions of protons on thin N_2 and O_2 targets at 12 GeV/c [8]. We compared the HARP data with the outputs of DPMJET-III and JAM in Fig. 1. In the figure, we combine N_2 and O_2 target data as the data for air target, assuming the composition of air to be 78.5% N_2 and 21.5% O_2. We also assume the inelastic cross section for proton and air nuclei interactions to be 300 mb. In the figure, we find that JAM shows slightly better agreement with the HARP experiment than DPMJET-III. Also the secondary spectra of JAM is higher than that of DPMJET-III at lower energies.

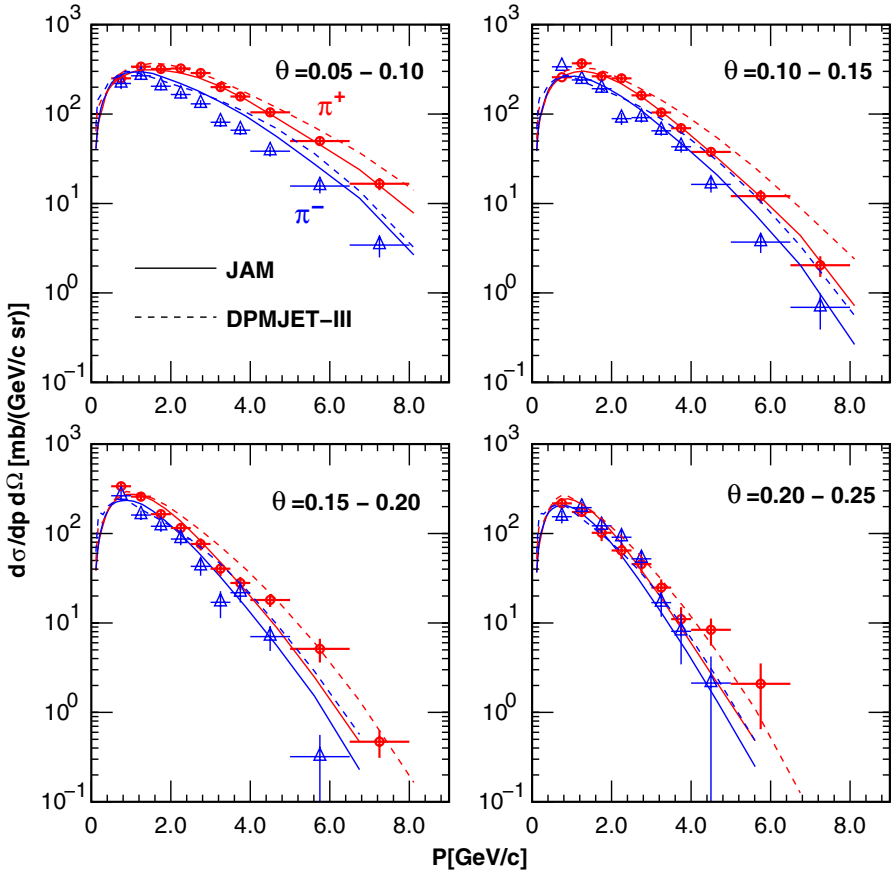

FIG. 1 (color online). Comparison of interaction models and HARP data. The solid lines stand for JAM, and the dashed lines for DPMJET-III.

Constructing the inclusive JAM, we calculate the atmospheric muon flux at the three different altitudes where the BESS group has carried out experimental studies of the atmospheric muon fluxes, at Tsukuba (30 m a.s.l.) [10], at Mt. Norikura (2770 m a.s.l.) [11], and at Fort Sumner (balloon altitudes) [12]. As the original JAM seems to have an upper limit for the projectile energy ($\lesssim 100$ GeV), we use it below 32 GeV. Above that energy we use the inclusive DPMJET-III, as the modified DPMJET-III reproduces the observed muon flux data above $\gtrsim 1$ GeV$/c$.

We show the comparisons of the calculations using the modified JAM with observations in Figs. 2–4, as the ratios of the observed muon fluxes to the calculated ones. In these calculations, we used the air density profile measured on the same date as the observations. This makes the agreement between the calculation and observation better for $\gtrsim$ 1 GeV$/c$. Some modifications are also applied to the JAM model, following the procedure explained in Appendix A.

We note that it was very difficult to modify the inclusive DPMJET-III only to give the muon flux as large as the observed one at Tsukuba and at Fort Sumner observed by BESS below 1 GeV$/c$. Introducing the inclusive JAM with the some modifications, we can boost the calculated muon flux below 1 GeV, and get good agreement between the calculations and observations at Tsukuba and Fort Sumner. However, boosting the muon flux below 1 GeV makes the difference between the calculation and observations at Mt. Norikura larger. We consider that it is more important to reduce the difference at balloon altitudes, since the atmospheric muon at the balloon altitude is directly related to the primary cosmic rays and the hadronic interactions at the energy relevant to the low energy ($\lesssim 1$ GeV) atmospheric neutrinos. We can carry out a study of the hadronic interaction at this energy as we did in the previous publication [4] using the muons observed at ground level at the energy relevant to the atmospheric neutrino with energies above 1 GeV. We calculate the atmospheric neutrino flux with the modified JAM in this paper.

In Fig. 5, we show the comparison of the x-spectra ($x \equiv E_{\text{secondary}}/E_{\text{projectile}}$) of the original JAM and the original DPMJET-III, and those of the modified JAM and the modified DPMJET-III which we actually used to calculate the fluxes in Figs. 2–4. In both panels, we find that JAM shows slightly higher spectra than DPMJET-III in $x \lesssim 0.2$. This is the reason for the higher atmospheric muon flux below 1 GeV$/c$ with the modified JAM. And, our modification method cannot modify DPMJET-III to have this high x-spectra for $x \lesssim 0.2$ and also keep the high spectra for $x \gtrsim 0.2$ required by the observed muon flux above 1 GeV.

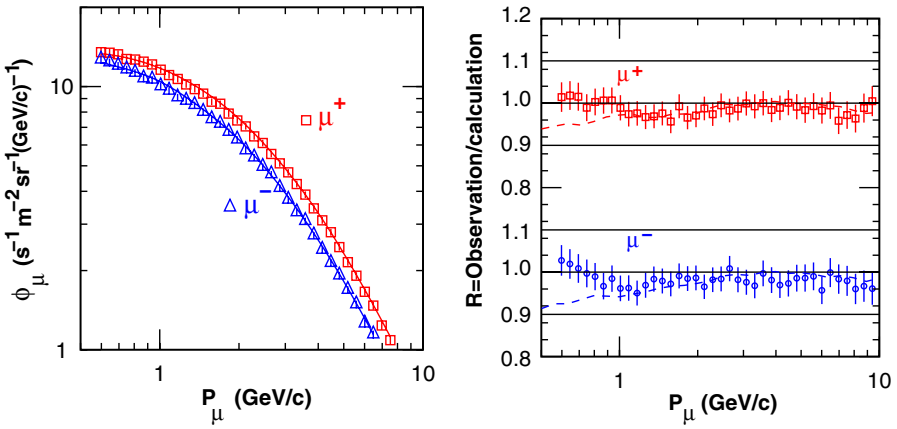

FIG. 2 (color online). Comparison of the muon flux observed at Tsukuba (30 m a.s.l.) and the one calculated with the modified JAM. Dashed lines in right panel are the ratios of former calculations to present ones.

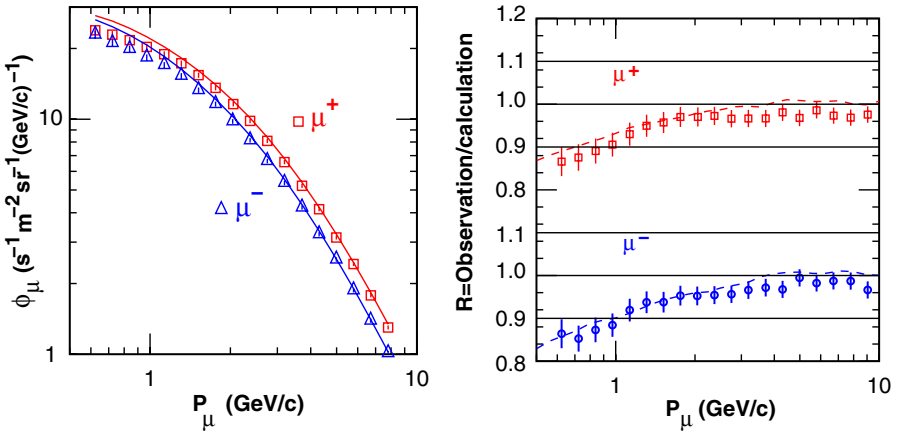

FIG. 3 (color online). Comparison of the muon flux observed at Mt. Norikura (2770 m a.s.l) and the one calculated with the modified JAM. Dashed lines in right panel are the ratios of former calculations to present ones.

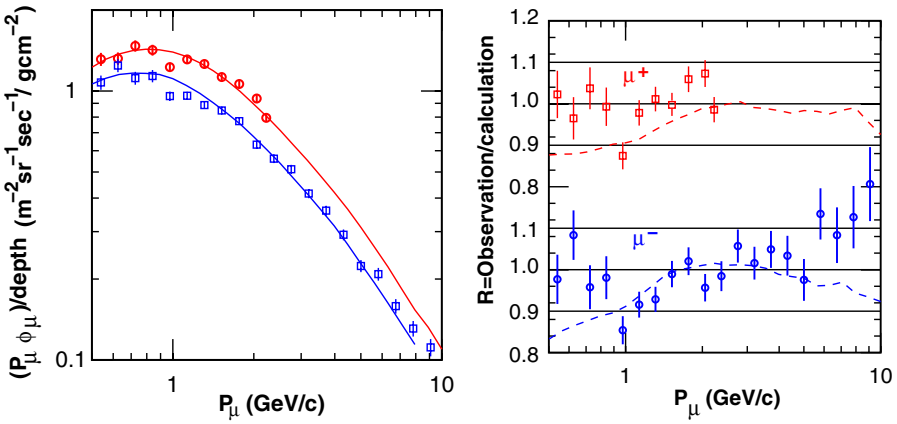

FIG. 4 (color online). Comparison of the muon flux observed at the balloon altitudes ($5 - 2$ g/cm^2) at Fort Sumner and the one calculated with the modified JAM. Dashed lines in right panel are the ratios of former calculations to present ones.

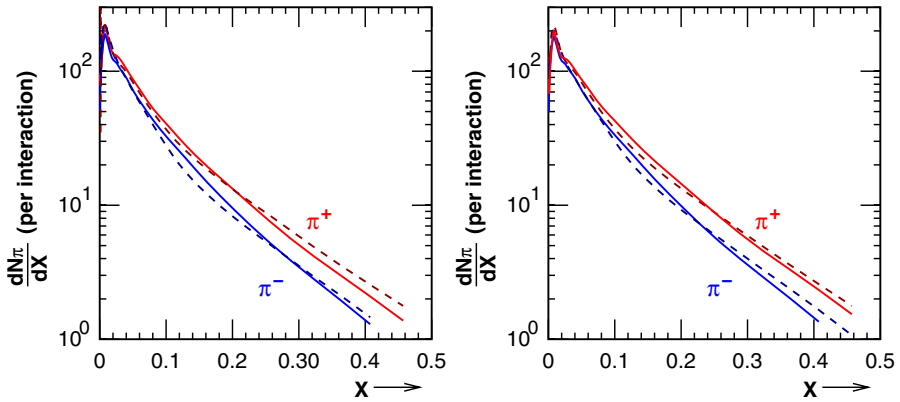

FIG. 5 (color online). Comparison of pion production spectra between the original JAM (solid line) and the original DPMJET-III (dashed line) integrated all over the directions in the left panel, and those of the modified JAM (solid line) and the modified DPMJET-III (dashed line) in the right panel at 10 GeV. Here the X denotes the ratio of secondary kinetic energy to projectile kinetic energy.

III. CALCULATION OF ATMOSPHERIC NEUTRINO FLUX

The scheme for calculating the atmospheric neutrino fluxes is almost the same as for the previous calculations [1,2], and so we only briefly review it here. We use the same primary flux model based on AMS [13,14] and BESS [10,15] data, with a spectral index of -2.71 above 100 GeV (see also Refs. [16,17]). We used the U.S.-standard '76 model of the atmosphere [18], as the error due to the atmospheric density model is sufficiently small for the calculation of atmospheric neutrino fluxes [1]. We use the IGRF2005 [19] geomagnetic model, as the variation due to changes of geomagnetic field would be small, and only extrapolation is available to the year 2010 at the time of computation.

For the 3D calculation of the atmospheric neutrino fluxes, we work in the Cartesian coordinate system which has the origin at the center of the Earth, with the Z-axis extending to the north pole, and we consider the surface of the Earth is a sphere with a radius of $R_e = 6378.180$ km. However, the position on the Earth is rather well represented by the spherical polar coordinate system (r, θ, ϕ) with $r = R_e$, related to the Cartesian coordinate system by

$$x = R_e \sin\theta \cos\phi,$$
$$y = R_e \sin\theta \sin\phi, \quad \text{and} \quad z = R_e \cos\theta a. \tag{1}$$

The local coordinate system at the detector is constructed based on this polar coordinate system. The direction of the x-axis is in the increasing direction of θ, the direction of the y-axis is in the increasing direction of ϕ, and the direction of the z-axis is in the increasing direction of r. Therefore, the azimuth angle is measured counterclockwise from south in the local coordinate system.

In addition to the surface of the Earth, we assume three more spheres; the injection sphere, the simulation sphere, and the escape sphere. In the previous work, we took the radius of the injection sphere as $R_{\rm inj} = R_e + 100$ km, the radius of simulation sphere as $R_{\rm sim} = R_e + 3000 = 9378.18$ km, and the escape sphere as $R_{\rm esc} = 10 \times R_e = 63781.80$ km. However, we take the radius of the simulation sphere to be $R_{\rm sim} = 10 \times R_e = 63781.80$ km, the same as the escape sphere, as a result of the increase in computation power. However, this change does not cause any visible difference in the results.

Cosmic rays are sampled on the injection sphere uniformly toward the inward direction, following the given primary cosmic ray spectra. Before they are fed to the simulation code for the propagation in air, they are tested to determine whether they pass the rigidity cutoff, i.e., the geomagnetic barrier. For a sampled cosmic ray, the "history" is examined by solving the equation of motion in the negative time direction. When the cosmic ray reaches the escape sphere without touching the injection sphere again in the inverse direction of time, the cosmic ray can pass through the magnetic barrier following its trajectory in the normal direction of time.

The propagation of cosmic rays is simulated in the space between the surface of Earth and the simulation sphere. When a particle enters the Earth, we discard the particle. Note, those particles which enter the Earth are mainly muons, and the number of muons which enter the Earth are far smaller than the number of muons which decay in air. Also, when muons enter the Earth, they lose energy quickly, and decay at rest or are captured by an atom in the rock and produce a neutrino with energies lower than 100 MeV.

Note, the neutrino detectors are very small compared with the size of the Earth, and are considered as infinitesimal points on the surface of the Earth. We need a finite size "virtual detector" instead of the infinitesimal neutrino detector in the 3D calculation of the atmospheric neutrino flux. However, the averaged neutrino flux in the finite size virtual detector is a little different from the neutrino flux at the actual neutrino detector, and we introduced the "virtual detector correction" in Ref. [1]. This virtual detector correction is refined in this paper.

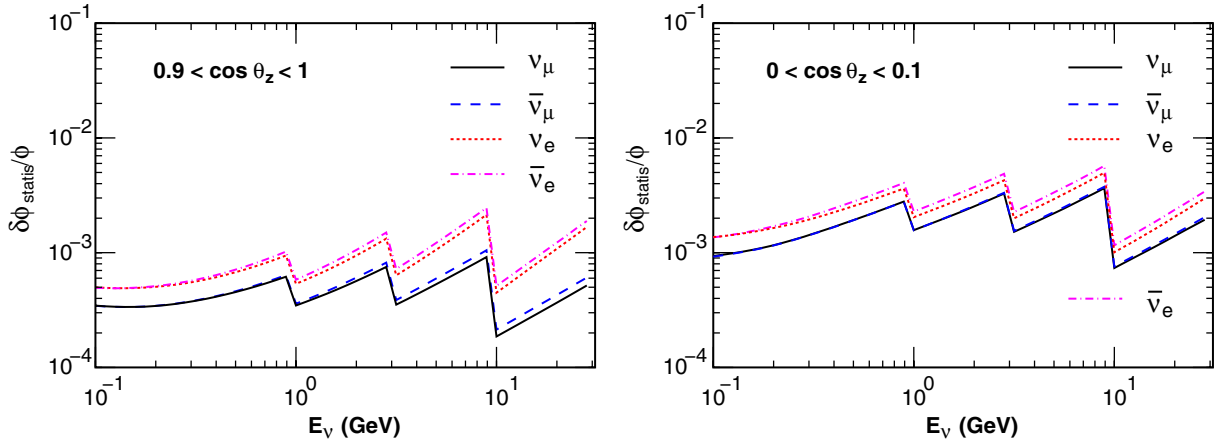

FIG. 6 (color online). The ratio of statistical errors of the atmospheric neutrino flux calculated to the flux value in this work. We show the statistical errors for near-vertical directions ($0.9 < \cos\theta_z < 1$) in the left panel, and for near-horizontal directions ($0.9 < \cos\theta_z < 1$) in the right panel, both averaging over all azimuthal directions.

The procedure for the correction is the same as in Ref. [1]. Using the inside of the circle with radius of θ_d as the virtual detector, the flux Φ_{θ_d} obtained with the virtual detector and the flux Φ_0 at the real target detector are related by

$$\Phi_{\theta_d} \simeq \Phi_0 + \Phi_0' \theta_d^2. \tag{2}$$

The term with Φ_0' may be cancelled out using two virtual detectors, with radii of θ_1 and θ_2, as

$$\Phi_0 \simeq \frac{\theta_1^2 \Phi_2 - \theta_2^2 \Phi_1}{\theta_1^2 - \theta_2^2} = \frac{\Phi_2 - r^2 \Phi_1}{1 - r^2}, \tag{3}$$

where we assumed $\theta_1 > \theta_2$.

In Appendix B, we study the ratio of the statistical errors $\Delta\Phi_0/\Delta\Phi_1$ as the function of r. We find that the ratio takes the minimum value $\sqrt{(5)} \simeq 2.236$ at $r = 1/\sqrt{2} \simeq 0.707$, whereas we took $r = 0.5$ in Ref. [1]. However, the ratio $\Delta\Phi_0/\Delta\Phi_1$ is a slowly varying function of r near the minimum, and the ratio at $r = 0.5$ is not too bad (2.517).

We take the radius of the virtual detector I as 1113.6 km corresponding to the angle from the center of the Earth of 10 degrees, as in Ref. [1], but we take the radius of the virtual detector II as 787.4 km corresponding to 7.071 degrees in this work. The virtual detector correction is applied up to $E_\nu = 10$ GeV, as we find a large difference in the fluxes determined by the virtual detectors I and II for some directions near the horizon (Fig. 17, in Appendix B).

In the previous work, we connected the atmospheric neutrino fluxes calculated in the 3D scheme to the one calculated in the 1D scheme at 10 GeV. In this work, we connected the 3D scheme calculation to the 1D scheme at 32 GeV, since we find a dipolelike variation of ν_e and $\bar{\nu}_\mu$ for horizontal directions due to the muon bending in the geomagnetic field at 10 GeV.

It is not efficient to calculate the atmospheric neutrino spectrum from 0.1 GeV to 32 GeV in one simulation, as the cosmic ray spectra are so steep. Therefore, we calculate the atmospheric neutrino flux limiting the lowest neutrino energy to 1 GeV, 3.16 GeV, 10 GeV, and 31.6 GeV, also limiting the lowest energy of primary cosmic ray to 1 GeV, 3.16 GeV, 10 GeV, and 31.6 GeV, respectively. The flux calculated in those simulations are combined into single atmospheric neutrino spectrum for each direction and each kind of neutrino.

We show the statistical error in this work for near-vertical directions and for near-horizontal directions averaging over all azimuth angles, in Fig. 6. For the horizontal directions, the opening angle of the virtual detector decrease with $\cos\theta$, where θ is the zenith angle. Therefore, the statistical error for near-horizontal directions is larger than that for near-vertical directions. The statistical error depends not only on the calculation scheme, but also on the analysis method of the simulation data. The analysis method of the simulation data and the estimation of the statistical error in our calculation is explained in Appendix C in some detail.

We find the statistical errors are well below 1% for the average over the azimuth angles. For each azimuth bin, however, the statistical errors reach a few percent for some directions. The largest statistical errors are found at the energy just below 10 GeV, due to the virtual detector correction applied up to this energy.

IV. ATMOSPHERIC NEUTRINO FLUXES CALCULATED WITH MODIFIED JAM

We show the calculated atmospheric neutrino fluxes with the modified JAM in this section. In the left panel of Fig. 7, the calculated atmospheric neutrino spectra are shown averaged over all directions from 0.1 GeV to 32 GeV for Kamioka, together with the ones calculated in our previous work, and those of the Bartol group [20,21], and the FLUKA group [22]. Above 32 GeV, the 3D

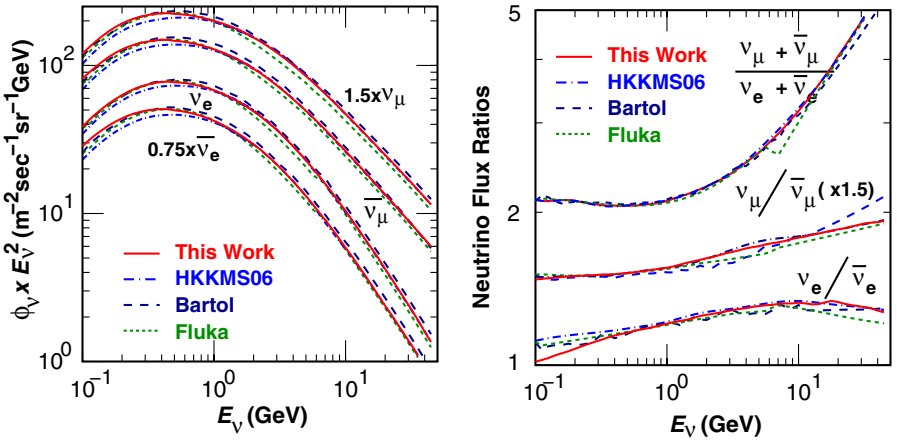

FIG. 7 (color online). Comparison of atmospheric neutrino fluxes calculated for Kamioka averaged over all directions (left panel), and the flux ratios (right panel), with other calculations. The dashed lines are the calculation by the Bartol group [20,21], dotted lines for the FLUKA group [22], and dash dot for our previous calculation (HKKM06).

calculation is smoothly connected to the 1D calculation carried out in the previous work. As the modified JAM is used below 32 GeV, any difference above that is due to the difference of the calculation scheme between 3D and 1D. However, the difference between present and previous works is very small in the figure above 1 GeV. Note, we magnify the difference between present and previous works in the ratio in Fig. 8. The difference is less than a few percent above 1 GeV. On the other hand, the atmospheric neutrino fluxes calculated with the modified-JAM show an increase from the previous one below 1 GeV, as is expected from the increase of atmospheric muon spectra below 1 GeV/c.

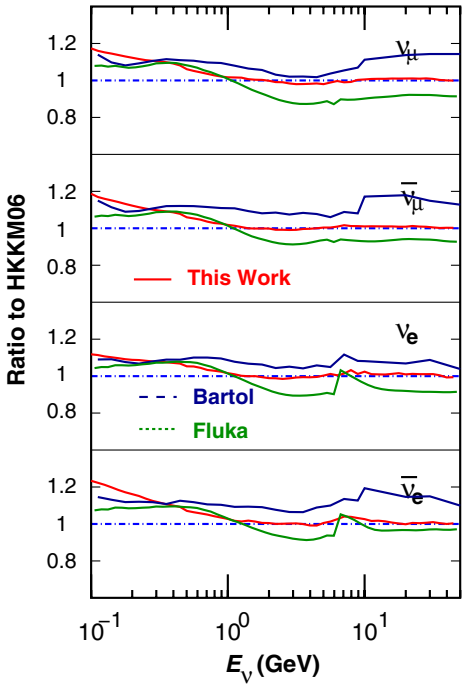

FIG. 8 (color online). Atmospheric neutrino fluxes calculated for Kamioka averaged over all directions, as a ratio to the HKKM06 calculation. The dashed lines are the calculation by Bartol group [20,21] and dotted lines the FLUKA group [22].

In the right panel of Fig. 7, we show the ratios of the atmospheric neutrino flux averaged over all directions. It is seen that the differences in the flux ratios are very small between present and previous works above 1 GeV as the absolute atmospheric neutrino fluxes. It is noticeable that the $(\nu_\mu + \bar{\nu}_\mu)/(\nu_e + \bar{\nu}_e)$ ratios are very close to each other including the ones calculated by different authors. We find there is a visible difference in $\nu_e/\bar{\nu}_e$ between the present and previous works. As is seen in the left panel of Fig. 5 in Sec. II, the original JAM interaction model has a smaller π^+/π^- ratio, and is responsible for the smaller $\nu_e/\bar{\nu}_e$ ratio below 1 GeV. Note, we do not modify the interaction model more than the muon flux data require. It is difficult to examine the μ^+/μ^- ratio at the momenta corresponding to the $\nu_e/\bar{\nu}_e$ below 1 GeV, due to the small statistics in the observation at balloon altitude.

The muons at sea level or mountain altitude are not useful to examine the atmospheric neutrino of these energies, since the muons result from higher energy pions at higher altitude.

In Fig. 9, we show the atmospheric neutrino fluxes as a function of the zenith angle averaging over all the azimuthal angles at 3 neutrino energies; 0.32, 1.0, and 3.2 GeV for Kamioka. In Fig. 10, we show the comparison of the present and previous works in the ratio as the function of zenith angle. There is a difference due to the increase of the neutrino flux itself, but the ratio is almost constant. Actually, the calculated zenith angle dependences are virtually the same as for the calculation in Ref. [2].

It seems that the zenith angle dependence of the 3D calculation is smoothly connected to that of the 1D calculation just above 3.2 GeV for the average over all azimuth angles. However, this is not true when we study

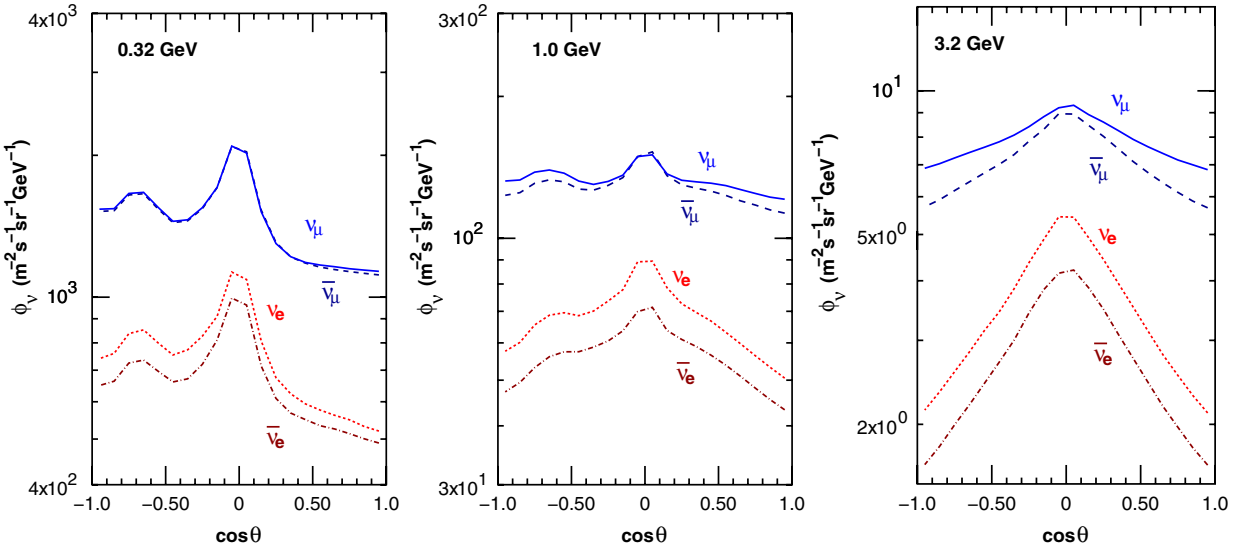

FIG. 9 (color online). The zenith angle dependence of atmospheric neutrino flux averaged over all azimuthal angles calculated for Kamioka. Here θ is the arrival direction of the neutrino, with $\cos\theta = 1$ for vertically downward going neutrinos, and $\cos\theta = -1$ for vertically upward going neutrinos.

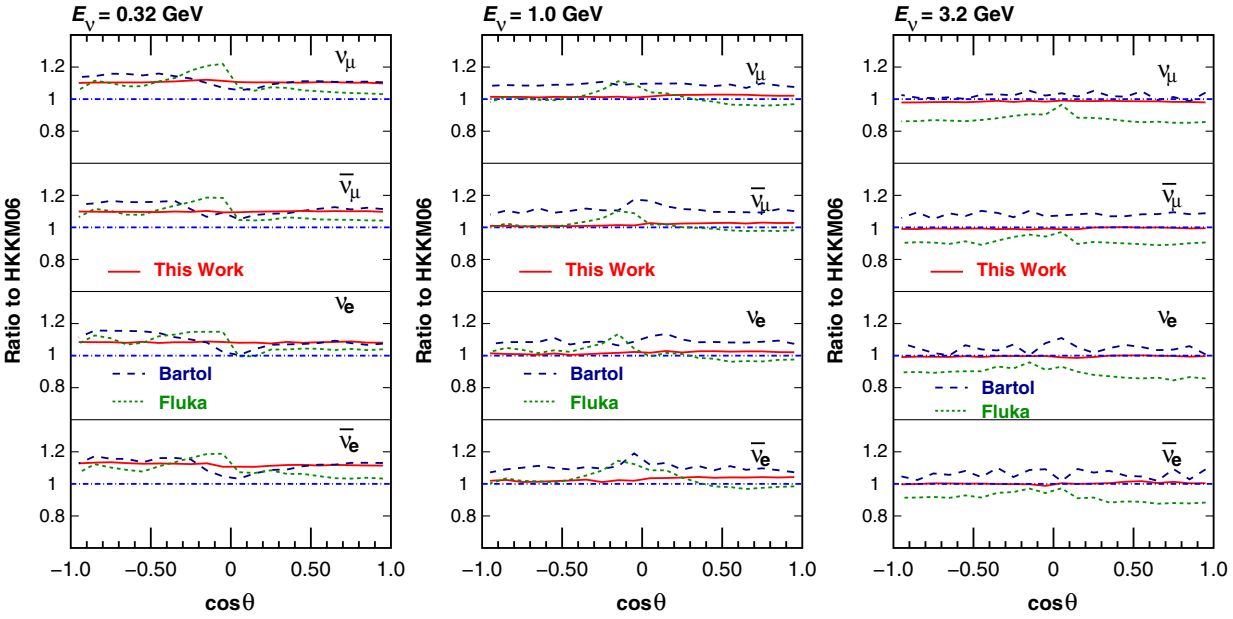

FIG. 10 (color online). Ratio of the atmospheric neutrino flux averaged over azimuth angles as the function of zenith angle to the same quantity calculated in HKKM06. The short dash lines stand for the calculation by Bartol group [20,21] and dotted lines for the FLUKA group [22].

the variation of atmospheric neutrino flux as a function of azimuthal angle. In Fig. 11, we show the variation of atmospheric neutrino flux as the function of the azimuthal angle averaging them over the five zenith angle ranges, $1 > \cos\theta > 0.6$, $0.6 > \cos\theta > 0.2$, $0.2 > \cos\theta > -0.2$, $-0.2 > \cos\theta > -0.6$, and $-0.6 > \cos\theta > -1$, at 1 GeV for Kamioka. It is seen in that the variation of the atmospheric neutrino flux has complex structures at 1 GeV due to the rigidity cutoff and muon bending in the geomagnetic field [23]. Note, the variation of upward going neutrinos ($-0.2 > \cos\theta$) is much more complicated than the variation of downward going neutrinos ($\cos\theta > 0.2$). This is because the upward-going neutrinos are produced in a far larger area on the Earth than the downward-going neutrinos, and are affected by large variation of rigidity cutoff and geomagnetic field. The downward-going neutrinos are produced just above the detector.

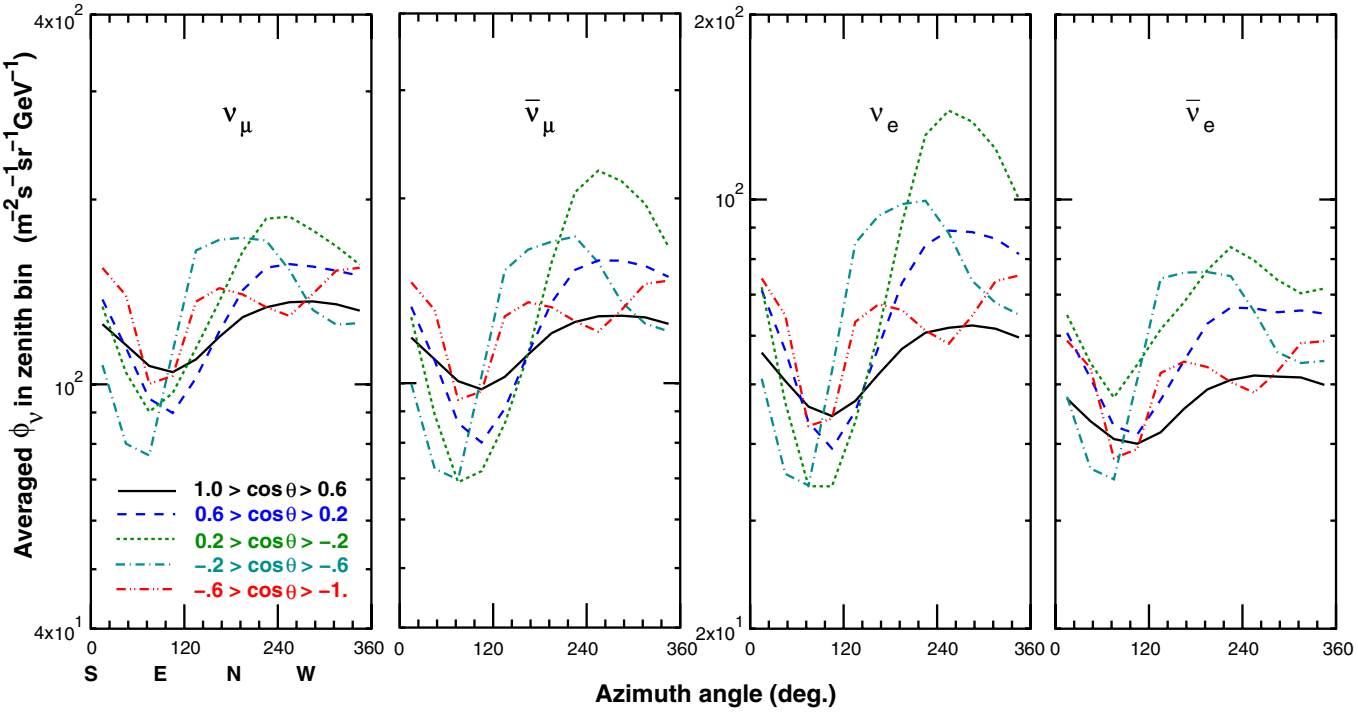

FIG. 11 (color online). The azimuthal angle dependence of atmospheric neutrino flux at 1 GeV, averaged over zenith angle bins of $1 > \cos\theta > 0.6$, $0.6 > \cos\theta > 0.2$, $0.2 > \cos\theta > -0.2$, $-0.2 > \cos\theta > -0.6$, and $-0.6 > \cos\theta > -1$ calculated for Kamioka.

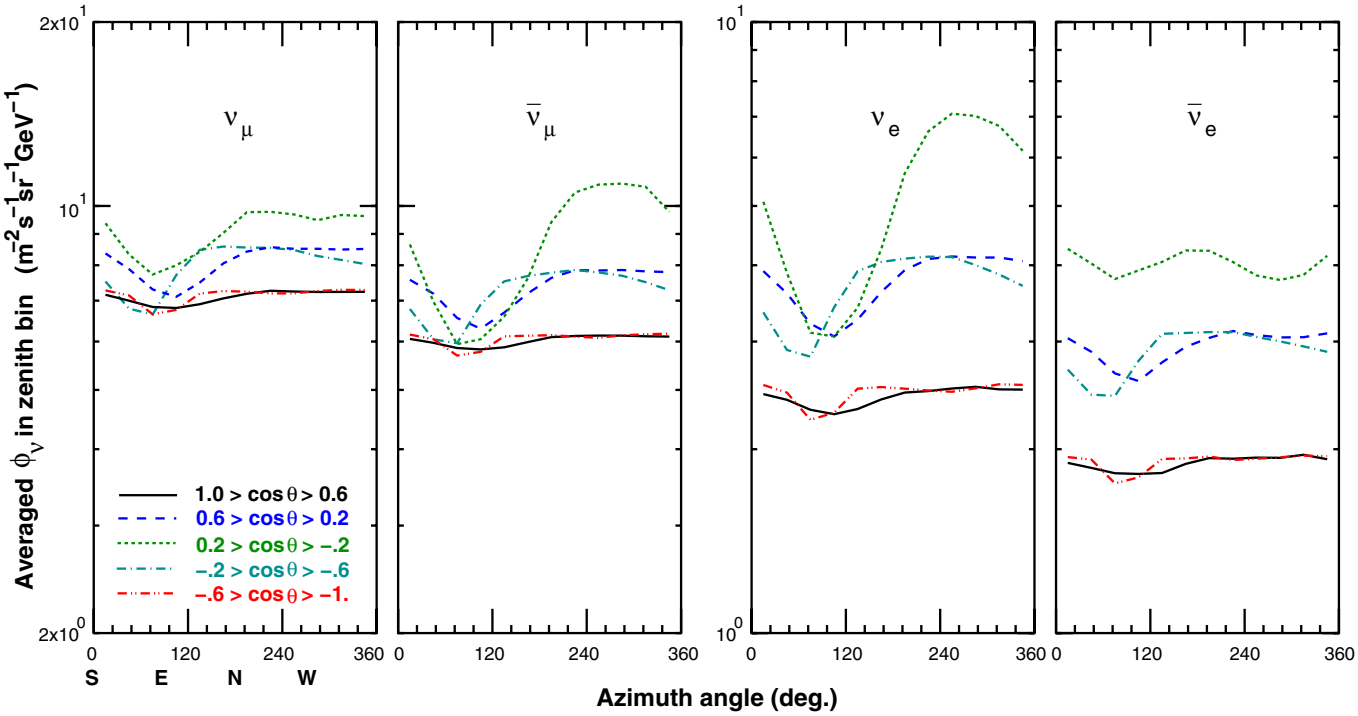

FIG. 12 (color online). The azimuthal angle dependence of atmospheric neutrino flux at 3.2 GeV, averaged over zenith angle bins of $1 > \cos\theta > 0.6$, $0.6 > \cos\theta > 0.2$, $0.2 > \cos\theta > -0.2$, $-0.2 > \cos\theta > -0.6$, and $-0.6 > \cos\theta > -1$ calculated for Kamioka.

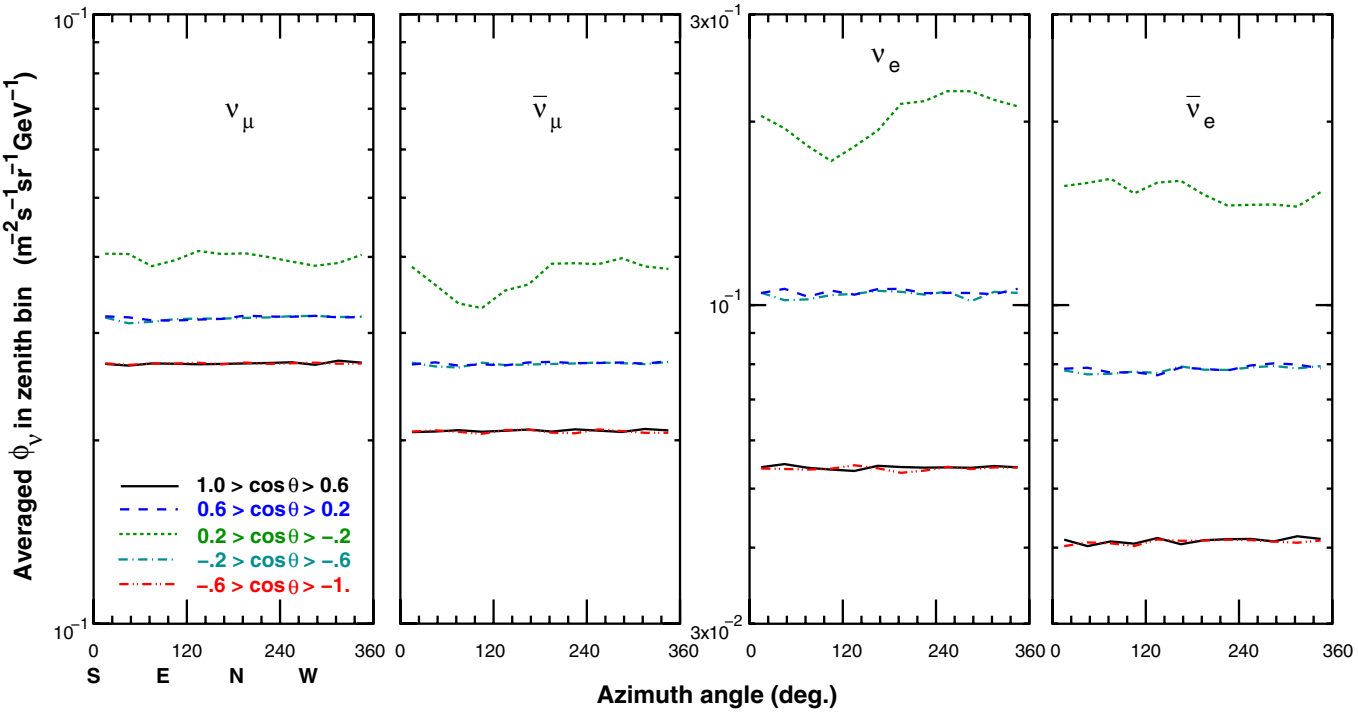

FIG. 13 (color online). The azimuthal angle dependence of atmospheric neutrino flux at 10 GeV, averaged over zenith angle bins of $1 > \cos\theta > 0.6$, $0.6 > \cos\theta > 0.2$, $0.2 > \cos\theta > -0.2$, $-0.2 > \cos\theta > -0.6$ and $-0.6 > \cos\theta > -1$ calculated for Kamioka.

In Fig. 12, we show the variation of atmospheric neutrino flux as the function of the azimuthal angle averaging them over the same five zenith angle bins at 3.2 GeV for Kamioka. At this neutrino energy, we find the deficit of neutrino flux due to the rigidity cutoff from the East direction ($\phi \sim 90°$) clearly for all kind of neutrinos and all zenith angle bins. However, the ν_e and $\bar{\nu}_\mu$ show large dipole structures in the horizontal zenith angle bin

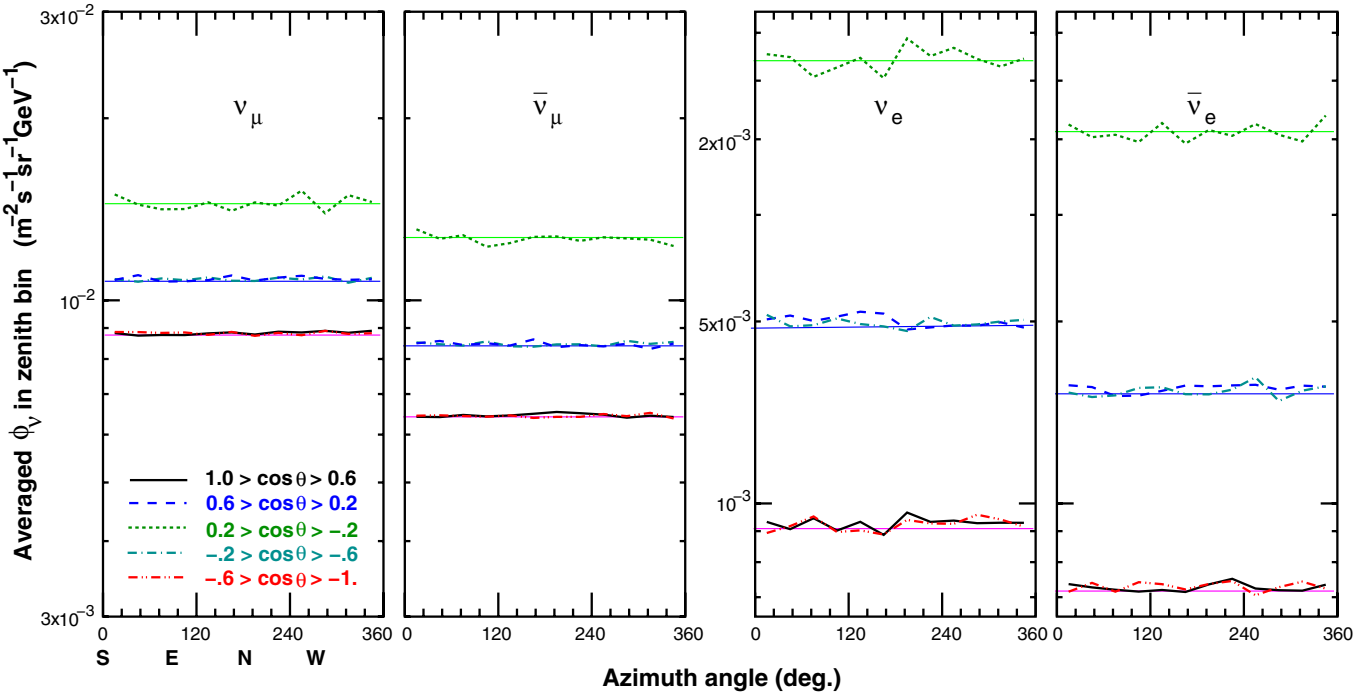

FIG. 14 (color online). The azimuthal angle dependence of atmospheric neutrino flux at 32 GeV, averaged over zenith angle bins of $1 > \cos\theta > 0.6$, $0.6 > \cos\theta > 0.2$, $0.2 > \cos\theta > -0.2$, $-0.2 > \cos\theta > -0.6$, and $-0.6 > \cos\theta > -1$ calculated for Kamioka. The straight lines in the figure show the flux values calculated in the 1D scheme.

$(0.2 > \cos\theta > -0.2)$ due to the muon bending in the geomagnetic field.

In Fig. 13, we show the variation of atmospheric neutrino flux as a function of the azimuthal angle averaging over the same five zenith angle bins at 10 GeV for Kamioka. At this energy, the atmospheric neutrinos seem to be free from the rigidity cutoff, but the ν_e and $\bar{\nu}_\mu$ still show the dipole structures in the horizontal zenith angle bin $(0.2 > \cos\theta > -0.2)$.

The dipole structure of ν_e and $\bar{\nu}_\mu$ seems to extend to a few 10 GeV in the horizontal bin. In Fig. 14, we show the variation of atmospheric neutrino flux as the function of the azimuthal angle averaging them over the same five zenith angle bins at 32 GeV calculated for Kamioka. We still see the dipole azimuth angle variation of ν_e at this energy in the horizontal bin. However, the amplitude of the variation is almost the same as that of the statistical error. Therefore, we connect the atmospheric neutrino flux calculated in the 3D scheme to the ones calculated in the 1D scheme at 32 GeV. In Fig. 14, we also plotted the flux vales calculated in the 1D scheme. We can say the flux values calculated in the 3D and 1D schemes agree within the statistical error, except for the dipole structure of ν_e in the horizontal bin.

V. SUMMARY AND DISCUSSION

After the previous publication, we have searched for an interaction model which has better behavior at low energies than DPMJET-III and NUCRIN, and we found that the JAM interaction model, used in PHITS (Particle and Heavy-Ion Transport code System) [6], shows slightly better agreement with the HARP experiment than DPMJET-III.

Constructing the inclusive interaction model from the JAM interaction model, we have used it as the hadronic interaction code in the simulation of cosmic ray propagation through the atmosphere below 32 GeV. Above this energy, we continue to use the modified DPMJET-III, since we could reproduce the result of atmospheric muon observations by BESS for $\gtrsim 1$ GeV/c in the previous work.

Applying some modifications to the inclusive JAM, we were able to increase the atmospheric muon flux below 1 GeV/c, and achieved better agreement with BESS observations at Tsukuba (30 m a.s.l.) and at Fort Sumner (balloon altitudes). However, the increase of the atmospheric muon flux below 1 GeV/c made the difference larger between calculation and observations at Mt. Norikura (2770 m a.s.l.). We consider the agreement at the balloon altitudes to be more important, since muons are observed there with almost the same momentum as they are produced. We then calculate the atmospheric neutrino fluxes with the modified-JAM as the hadronic interaction code below 32 GeV.

The calculation scheme is essentially the same as in previous calculations, but the radius of the simulation sphere has been made the same as that of the escape sphere, to reduce the boundary effect. However, there is no visible effect from this change in the calculated atmospheric neutrino fluxes. Also we revised the formula for the size correction of the virtual detector to minimize the statistical errors, which were reduced by $\sim 11\%$.

Some features of the calculated atmospheric neutrino flux are presented in section IV. The use of the modified-JAM increased the atmospheric neutrino fluxes below 1 GeV corresponding to the increase of atmospheric muon fluxes below 1 GeV/c. However, the ratios of the atmospheric neutrinos, especially $(\nu_\mu + \bar{\nu}_\mu)/(\nu_e + \bar{\nu}_e)$, are very close to the previous calculation. Only the ratio $\nu_e/\bar{\nu}_e$ shows a decrease near 0.1 GeV due to the small π^+/π^- ratio of the original JAM. It is difficult to study the π^+/π^- ratio from the observed atmospheric muons. Also the zenith angle variations of the atmospheric neutrinos are virtually the same as the previous calculations.

The azimuth angle variations of the atmospheric neutrino fluxes are studied in detail in this paper. For horizontal directions $(0.2 > \cos\theta > -0.2)$, $\bar{\nu}_\mu$ and ν_e still show a dipolelike variation even at 10 GeV due to the deflections of muons in the geomagnetic field. However, the magnitude of the variation become almost the same as the statistical error at 32 GeV even for horizontal directions. As a result, we connected the atmospheric neutrino fluxes calculated in the 3D calculation scheme to those calculated in the 1D calculation scheme at 32 GeV. They agree with each other within the statistical error at this energy.

The study of the interaction model and atmospheric muons, similar to that in the previous publication, suggests that the magnitude of the error of the atmospheric neutrino flux due to the hadronic interaction model at energies below 1 GeV is similar to the maximum difference between the calculated atmospheric muon fluxes and observed ones below $\lesssim 3$ GeV/c at balloon altitudes. Assuming $\sim 10\%$ of the uncertainty for the total interaction cross section of cosmic rays and air nuclei, or the interaction mean free path of the cosmic rays, we estimate the uncertainty of the atmospheric neutrino flux below 1 GeV is around 15% at 0.3 GeV, and 20% at 0.1 GeV.

ACKNOWLEDGMENTS

We greatly appreciate the contributions of J. Nishimura and A. Okada to this paper. We are grateful to T. Sanuki, K. Abe, and P. G. Edwards for discussions and comments. We also thank the ICRR of the University of Tokyo, especially for the use of the computer system.

APPENDIX A: INTERACTION MODEL AND CALCULATION OF ATMOSPHERIC NEUTRINO FLUX

Here, we explain the construction of the inclusive code from the output of the original interaction code. First we

ran the original code many times, and recorded the kind, energy, and momentum of the secondary particle. We sort and number them in the ascending order of $x \equiv E_{\rm secondary}/E_{\rm projectile}$ as

$$x_1 < \cdots < x_{i-1} < x_i < x_{i+1} < \cdots < x_n, \tag{A1}$$

for each kind of secondary particle. Considering this series as a function of integer in $[1, n]$, we can define a function of a discrete variable in (0,1] as

$$x_i = X\left(\frac{i}{n}\right). \tag{A2}$$

This $X(i/n)$ converges to a continuous function in [0, 1] as the number of trials, or n, increases, and the asymptotic continuous function can be approximated by a proper fitting function for sufficiently large n.

Writing the asymptotic function also as $X(u)$, we can generate the x following the x-distribution of the original interaction model with uniform random numbers u in [0, 1] as

$$x = X(u). \tag{A3}$$

It is straightforward to calculate the energies of the secondary particles from x.

As the fitting function, we used the B-spline function for DPMJET-III and NUCRIN, but we take the poly-quadra function for JAM for accuracy, although the difference in the actual usage is small.

We fit the angular distribution by the fitting formula,

$$F(\cos\theta)d\cos\theta = \exp(A + a(\cos\theta + 1)^{\alpha}(1 - \cos^2\theta)^{\beta})d\cos\theta, \tag{A4}$$

at low energies ($\lesssim 32$ GeV). We determine the parameters, A, a, α, and β for each x-bin with $\log\Delta x = 0.1$. For higher energies, we fit the angular distribution with a simple formula

$$F'(\cos\theta)d\cos\theta = \exp(A + a \cdot \cos\theta)d\cos\theta, \tag{A5}$$

which is a special case of Eq. (A4).

Repeating the above procedures for all kinds of secondary particle and for all the projectile energy grids, the inclusive code is constructed for the interaction model. Note, the projectile energy grids are selected to cover the required projectile energy range. For the projectile energy in between two energy grids, we use the set of parameters at either grid energy. The grid energy to use is determined by the distances to both grid energies and a random number in a probabilistic way.

As the grid projectile energies, we took $\log(E_g/1\ \text{GeV}) = 0.5,\ 1.0\ \ldots\ 5.5$, and 6.0 for DPMJET-III, and $\log(E_g/1\ \text{GeV}) = -0.7, -0.6, -0.4, 0.0$, and 0.5 for NUCRIN. For the JAM interaction model, we take $\log(E_g/1\ \text{GeV}) = -1, -0.9, \ldots 0., 0.1, \ldots 1.6$, and 1.7.

As noted previously, the inclusive code allows us to readily modify the secondary spectra of the original interaction model. When we apply a modification to the inclusive code, we replace the uniform random generator to the weighted random number generator in [0, 1], instead of the uniform random number generator. We take a simple form for the weight function,

$$w_i(u) = 1 + a_i \cdot u, \tag{A6}$$

and request the random numbers are generated in the probability proportional to $w(u)$. The a_i are the modification parameters defined at the projectile energy grid for all the kind of secondary particles. At each projectile energies, the a_i are not independent but the total energy of secondary particle is conserved on average. The multiplicities are not modified.

The above modification procedure is an effective way to modify so called Z-factor ($Z \equiv \langle x^{1.7}\rangle$, with $x \equiv E_{\rm secondary}/E_{\rm projectile}$) which is a good description for atmospheric muons and neutrinos at high energies [9].

APPENDIX B: VIRTUAL DETECTOR CORRECTION AND THE OPTIMIZATION

We have shown in Ref. [1] that the average flux (Φ_{θ_d}) in a virtual detector with radius of θ_d is expressed as

$$\Phi_{\theta_d} \simeq \Phi_0 + \Phi_0'\theta_d^2, \tag{B1}$$

where Φ_0 is the atmospheric neutrino flux at the target detector, and Φ_0' is a constant determined for the target detector.

As in Ref. [1], we may cancel out the term with Φ_0' using two averaged fluxes in two concentric virtual detectors around the target detector. Assuming two virtual detectors with radii θ_1 and θ_2, we can calculate the flux at the target detector (Φ_0) as

$$\Phi_0 \simeq \frac{\theta_1^2\Phi_2 - \theta_2^2\Phi_1}{\theta_1^2 - \theta_2^2} = \frac{\Phi_2 - r^2\Phi_1}{1 - r^2}, \tag{B2}$$

where Φ_1 is the averaged flux in the virtual detector I with a radius of θ_1, and Φ_2 is the averaged flux in the virtual detector II with a radius of θ_2. Here, we assumed $\theta_1 > \theta_2$.

The treatment of the virtual detector in Ref. [1] corresponds to taking $r = 0.5$ in 3. However, this value is not optimal for the statistical error due to fluctuations in the number of neutrinos observed in the virtual detector. The fluxes Φ_1 and Φ_2 are calculated as

$$\Phi_1 = \frac{N_1}{T\pi\theta_1^2}, \quad \text{and} \quad \Phi_2 = \frac{N_2}{T\pi\theta_2^2},$$

where T is the corresponding observation time of the simulation, and N_1 and N_2 are the observed numbers of neutrinos in the virtual detectors I and II, respectively. The "true" flux Φ_0 is calculated from N_1 and N_2 as

$$\Phi_0 = \frac{1}{T\pi\theta_1^2 \cdot (1-r^2)}\left(\frac{N_2}{r^2} - r^2 N_1\right) \tag{B3}$$

We note that the neutrino observed by the virtual detector II is also observed by virtual detector I, therefore, $N_1 - N_2$ and N_2 are independent variables rather than N_1 and N_2. Therefore, in terms of independent variables, the true flux Φ_0 is rewritten as

$$\Phi_0 = \frac{1}{T\pi\theta_1^2 \cdot (1-r^2)}\left(\left(\frac{1}{r^2} - r^2\right)N_2 - r^2(N_1 - N_2)\right). \tag{B4}$$

Assuming Poissonian fluctuations for the numbers of the observed neutrinos, we can estimate the statistical error of the true flux as

$$\Delta\Phi_0 = \frac{1}{T\pi\theta_1^2 \cdot (1-r^2)} \times \sqrt{\left(\left(\frac{1}{r^2} - r^2\right)^2 r^2 + r^4(1-r^2)\right)N_1}, \tag{B5}$$

where we used the approximate relations $N_2 \simeq r^2 N_1$ and $N_1 - N_2 \simeq (1-r^2)N_1$. Therefore, the ratio of $\Delta\Phi_0/\Delta\Phi_1$ is given as

$$\frac{\Delta\Phi_0}{\Delta\Phi_1} = \frac{1}{1-r^2}\sqrt{\left(\frac{1}{r^2} - r^2\right)^2 r^2 + r^4(1-r^2)} \equiv F(r). \tag{B6}$$

The function $F(r)$ has a minimum at $r = 1/\sqrt{2} \simeq 0.707$ and $F(1/\sqrt{2}) = \sqrt{(5)} \simeq 2.236$ (Fig. 15). We take the radius of the virtual detector I as 1113.6 km corresponding to an angle of 10° at the center of the Earth, and the radius of the virtual detector II as 787.4 km corresponding to 7.071°.

The virtual detector correction is studied in the [before/after] ratio in our calculation for Kamioka in Fig. 16, for $1 > \cos\theta_z > 0.9$ as the near-vertical directions and for $0.1 > \cos\theta_z > 0$ as the near-horizontal directions, where θ_z is the arrival zenith angle. Note, the virtual detector correction is necessary and effective for the downward-going neutrinos [1].

From the figures, we find the virtual detector correction is needed below 3 GeV even for the average over all azimuth directions. When we divide all the arrival azimuth

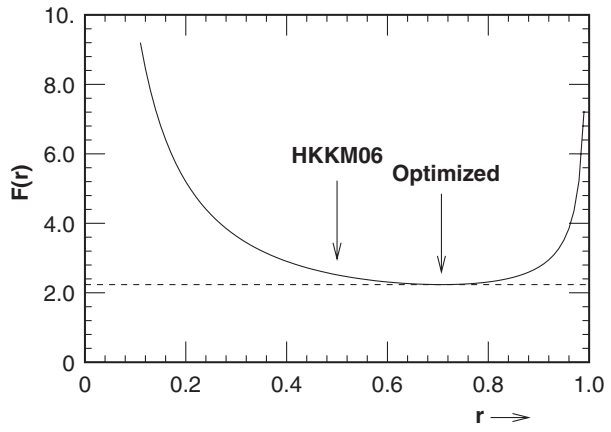

FIG. 15. The variation of the function $F(r)$ defined by (B6). It has a minimum value $\sqrt{5} \simeq 2.236$ at $r = 1/\sqrt{2} \simeq 0.707$ indicated by "Optimized." The "HKKM06" indicates the $r = 0.5$ used in HKKM06, where the F-value is a little larger than the optimized one ($F(0.5) = 2.517$).

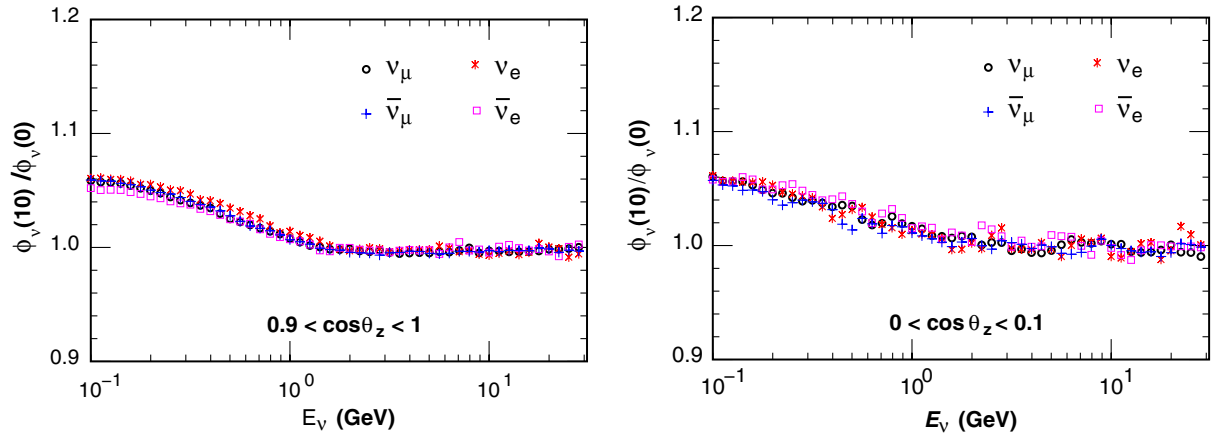

FIG. 16 (color online). Ratio of the atmospheric neutrino flux averaged over the virtual detector ($\phi(10)$) to the flux for the true neutrino detector ($\phi(0)$) estimated with the procedure explained in the text. The atmospheric neutrino fluxes are averaged over all the azimuth angles. Here, θ_z stands for the zenith angle of the arrival direction, and the left panel is for the near-vertical downward directions, and the right panel for the near-horizontal directions.

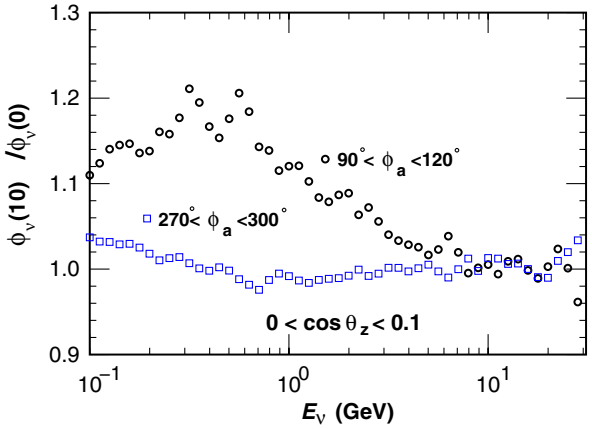

FIG. 17 (color online). Ratio of the neutrino fluxes averaged over the virtual detector ($\phi(10)$) to the flux for the true neutrino detector ($\phi(0)$) calculated with the procedure explained in the text for near-horizontal east ($90° < \phi_a < 120°$) directions.

angles into 12 bins, we find the largest correction in the azimuth bin of [90°, 120°] for near-horizontal directions ($0.1 > \cos\theta_z > 0$). Note, we measure the azimuth angle counterclockwise from south. We show the [before/after] ratio of the flux for this bin and opposite azimuth bin ([270°, 300°]) in Fig. 17, summing over all kinds of neutrino.

APPENDIX C: ANALYSIS OF SIMULATION DATA AND THE STATISTICAL ERROR

To analyze the simulation output, we take a logarithmically equally-spaced grid E_i for the neutrino energy as

$$E_i = E_0 \cdot R^i, \qquad (i = \ldots, -1, 0, 1, \ldots.), \tag{C1}$$

and count the numbers of neutrinos falling in each $[E_{i+1}, E_i]$ bin for each kind of neutrino and each arrival direction window. Note, we take $E_0 = 0.1$ GeV and $R = 10^{1/20}$, then used grids with $i \geq -1$ in this study. As usual, we assume that the integration of the neutrino flux in an energy bin is related to the number of neutrino in the bin as

$$I_i = \int_{E_i}^{E_{i+1}} \Phi(E) dE = \frac{N_i}{S \cdot \Omega \cdot T}, \tag{C2}$$

where N_i is the number of neutrinos in the $[E_{i+1}, E_i]$ bin, T is the equivalent time of the simulation, Ω is the opening angle of the window, and S is the area of the virtual detector.

We calculate the neutrino flux Φ_i at energy E_i from I_i and I_{i-1} which are integral fluxes calculated from the simulation in the two adjacent energy bins $[E_{i+1}, E_i]$ and $[E_i, E_{i-1}]$, respectively. For these two energy bins, we approximate the neutrino flux as the power function of the energy as $\Phi(E) = A \cdot E^\alpha$, and Φ_i is calculated as

$$\Phi_i = \frac{I_i I_{i-1}(\ln(I_i) - \ln(I_{i-1}))}{E_i \ln(R)(I_i - I_{i-1})}. \tag{C3}$$

This expression is singular at $I_i = I_{i-1}$, but it becomes a smooth function of I_i and I_{i-1}, if we define the value at $I_i = I_{i-1}$ as

$$\Phi_i = \frac{I_i}{E_i \ln(R)}, \tag{C4}$$

to which (C3) approaches in the $I_i \to I_{i-1}$ limit.

Assuming Poissonian fluctuations for the statistical error, the error for integrated flux $\Delta I_i / I_i$ is given by $1/\sqrt{N_i}$. The statistical error for Φ_i is estimated substituting (C3) into the general expression

$$\Delta\Phi_i = \sqrt{\left(\frac{\partial\Phi_i}{\partial I_i}\Delta I_i\right)^2 + \left(\frac{\partial\Phi_i}{\partial I_{i-1}}\Delta I_{i-1}\right)^2}, \tag{C5}$$

and the ratio $\Delta\Phi_i/\Phi_i$ is given as

$$\frac{\Delta\Phi_i}{\Phi_i} = \sqrt{\left(\frac{1}{\ln x} - \frac{1}{x-1}\right)^2 \frac{1}{N_i} + \left(\frac{1}{\ln(1/x)} - \frac{1}{1/x - 1}\right)^2 \frac{1}{N_{i-1}}}, \tag{C6}$$

where $x = I_i/I_{i-1} = N_i/N_{i-1}$. This expression is well-approximated by the simpler relation,

$$\frac{\Delta\Phi_i}{\Phi_i} \simeq \frac{1}{2}\sqrt{\frac{1}{N_i} + \frac{1}{N_{i-1}}}. \tag{C7}$$

In the $N_i \to N_{i-1}$ limit, both (C6) and (C7) give $1/\sqrt{N_1 + N_2}$, and the differences between them are less than 5% for $0.5 < N_i/N_{i-1} < 2$.

APPENDIX D: ATMOSPHERIC NEUTRINO FLUX BELOW 32 GEV

Here, we tabulate the atmospheric neutrino flux for solar minimum at sea level at locations—Kamioka, Sudbury (North America), and Gran Sasso—as in the former publication, averaging them over all the arrival azimuth directions and in the zenith angle bins with $\Delta\cos\theta_z = 0.1$, where θ_z is the zenith angle of the arrival direction of the neutrino, in Tables I, II, III, IV, V, VI, VII, VIII, IX, X, XI, XII, XIII, XIV, XV, XVI, XVII, XVIII, XIX, and XX.

Because of page limitations, we cannot present all the calculated results here. The atmospheric neutrino fluxes for different solar activity for Kamioka, Sudbury, Soudan2 site, Gran Sasso, Frejus, and Homestake will be available at http://www.icrr.u-tokyo.ac.jp/~mhonda.

TABLE I. Neutrino flux ($m^{-2}\,sec^{-1}\,sr^{-1}\,GeV^{-1}$) for $1.0 \geq \cos\theta_z > 0.9$.

	Kamioka				Sudbury				Gran Sasso				
E_ν (GeV)	ν_μ	$\bar{\nu}_\mu$	ν_e	$\bar{\nu}_e$	ν_μ	$\bar{\nu}_\mu$	ν_e	$\bar{\nu}_e$	ν_μ	$\bar{\nu}_\mu$	ν_e	$\bar{\nu}_e$	Norm
0.1000	4.25	4.25	2.02	2.08	11.91	12.05	6.01	5.34	7.34	7.43	3.56	3.51	10^3
0.1259	3.52	3.52	1.66	1.68	9.53	9.58	4.76	4.17	6.01	6.08	2.90	2.81	10^3
0.1585	2.81	2.81	1.31	1.31	7.27	7.27	3.60	3.09	4.74	4.77	2.26	2.14	10^3
0.1995	21.50	21.50	9.98	9.81	52.12	51.97	25.95	21.84	35.54	35.52	16.86	15.69	10^2
0.2512	15.68	15.68	7.32	7.04	35.16	34.99	17.80	14.63	25.33	25.16	12.03	10.97	10^2
0.3162	11.02	11.02	5.13	4.84	22.53	22.42	11.51	9.32	17.23	17.02	8.21	7.30	10^2
0.3981	7.46	7.46	3.47	3.21	13.86	13.68	7.09	5.66	11.26	11.04	5.35	4.65	10^2
0.5012	4.88	4.88	2.26	2.05	8.21	8.04	4.15	3.29	7.07	6.87	3.33	2.85	10^2
0.6310	3.09	3.09	1.42	1.26	4.74	4.57	2.35	1.85	4.29	4.11	2.00	1.67	10^2
0.7943	18.93	18.93	8.65	7.54	26.66	25.42	12.87	10.06	25.21	23.81	11.52	9.44	10^1
1.0000	11.31	11.31	5.06	4.32	14.92	13.96	6.84	5.34	14.46	13.45	6.42	5.15	10^1
1.2589	6.55	6.55	2.87	2.40	8.28	7.56	3.56	2.78	8.15	7.43	3.45	2.73	10^1
1.5849	3.70	3.70	1.58	1.29	4.56	4.06	1.83	1.42	4.53	4.02	1.80	1.41	10^1
1.9953	20.28	20.28	8.36	6.67	24.64	21.39	9.19	7.12	24.55	21.38	9.17	7.09	10^0
2.5119	10.83	10.83	4.25	3.36	13.16	11.16	4.54	3.48	13.16	11.17	4.53	3.47	10^0
3.1623	5.68	5.68	2.11	1.64	6.95	5.75	2.18	1.67	6.95	5.76	2.18	1.67	10^0
3.9811	29.33	29.33	10.13	7.77	36.42	29.46	10.28	7.85	36.45	29.54	10.32	7.85	10^{-1}
5.0119	15.07	15.07	4.76	3.62	18.95	15.04	4.80	3.64	18.99	15.06	4.79	3.64	10^{-1}
6.3096	7.65	7.65	2.19	1.66	9.78	7.62	2.19	1.67	9.80	7.64	2.20	1.67	10^{-1}
7.9433	38.61	38.61	9.94	7.52	50.15	38.59	9.86	7.52	50.20	38.63	9.87	7.53	10^{-2}
10.000	19.36	19.36	4.43	3.37	25.50	19.37	4.43	3.37	25.50	19.34	4.43	3.37	10^{-2}
12.589	9.70	9.70	1.97	1.50	12.94	9.71	1.97	1.50	12.93	9.70	1.97	1.50	10^{-2}
15.849	48.46	48.46	8.68	6.71	65.41	48.57	8.70	6.72	65.45	48.56	8.70	6.70	10^{-3}
19.953	24.26	24.26	3.84	2.99	33.06	24.31	3.84	2.99	33.02	24.29	3.84	3.00	10^{-3}
25.119	12.07	12.07	1.71	1.33	16.58	12.09	1.71	1.33	16.62	12.08	1.70	1.34	10^{-3}
31.623	60.83	60.83	7.68	6.08	84.16	60.73	7.67	6.08	84.27	60.79	7.66	6.06	10^{-4}

TABLE II. Neutrino flux ($m^{-2}\,sec^{-1}\,sr^{-1}\,GeV^{-1}$) for $0.9 \geq \cos\theta_z > 0.8$.

	Kamioka				Sudbury				Gran Sasso				
E_ν (GeV)	ν_μ	$\bar{\nu}_\mu$	ν_e	$\bar{\nu}_e$	ν_μ	$\bar{\nu}_\mu$	ν_e	$\bar{\nu}_e$	ν_μ	$\bar{\nu}_\mu$	ν_e	$\bar{\nu}_e$	Norm
0.1000	4.33	4.33	2.06	2.11	12.25	12.38	6.17	5.50	7.50	7.61	3.65	3.59	10^3
0.1259	3.57	3.57	1.69	1.71	9.71	9.76	4.87	4.27	6.12	6.18	2.95	2.86	10^3
0.1585	2.84	2.84	1.33	1.33	7.37	7.38	3.68	3.17	4.81	4.83	2.30	2.19	10^3
0.1995	21.65	21.65	10.20	9.94	52.72	52.62	26.52	22.35	35.98	35.94	17.24	15.99	10^2
0.2512	15.80	15.80	7.47	7.17	35.57	35.44	18.22	15.02	25.60	25.49	12.32	11.24	10^2
0.3162	11.09	11.09	5.27	4.95	22.84	22.72	11.84	9.59	17.48	17.27	8.45	7.51	10^2
0.3981	7.53	7.53	3.58	3.30	14.09	13.95	7.32	5.87	11.41	11.22	5.54	4.82	10^2
0.5012	4.94	4.94	2.34	2.12	8.36	8.22	4.33	3.43	7.19	7.00	3.48	2.96	10^2
0.6310	3.13	3.13	1.48	1.31	4.82	4.69	2.47	1.94	4.38	4.21	2.10	1.75	10^2
0.7943	19.26	19.26	9.03	7.89	27.38	26.25	13.54	10.64	25.78	24.48	12.18	9.99	10^1
1.0000	11.52	11.52	5.33	4.56	15.29	14.43	7.27	5.68	14.82	13.87	6.82	5.49	10^1
1.2589	6.68	6.68	3.04	2.54	8.48	7.83	3.82	2.97	8.36	7.69	3.69	2.92	10^1
1.5849	3.78	3.78	1.68	1.38	4.68	4.20	1.97	1.54	4.63	4.17	1.94	1.52	10^1
1.9953	20.80	20.80	8.94	7.20	25.31	22.26	9.98	7.73	25.26	22.14	9.91	7.68	10^0
2.5119	11.19	11.19	4.63	3.65	13.49	11.60	4.95	3.81	13.48	11.60	4.94	3.79	10^0
3.1623	5.88	5.88	2.30	1.79	7.14	5.99	2.40	1.83	7.15	6.00	2.40	1.83	10^0
3.9811	30.44	30.44	11.14	8.58	37.40	30.66	11.36	8.65	37.50	30.73	11.38	8.67	10^{-1}
5.0119	15.63	15.63	5.28	4.00	19.46	15.68	5.31	4.03	19.47	15.70	5.33	4.01	10^{-1}
6.3096	7.94	7.94	2.43	1.84	10.03	7.93	2.44	1.84	10.03	7.97	2.45	1.84	10^{-1}
7.9433	40.20	40.20	11.05	8.38	51.52	40.26	11.04	8.43	51.69	40.13	11.17	8.45	10^{-2}
10.000	20.11	20.11	4.98	3.77	26.17	20.12	4.96	3.76	26.21	20.10	4.97	3.76	10^{-2}
12.589	10.08	10.08	2.21	1.68	13.28	10.07	2.21	1.68	13.30	10.09	2.21	1.69	10^{-2}
15.849	50.50	50.50	9.77	7.51	67.24	50.40	9.77	7.48	67.29	50.42	9.74	7.50	10^{-3}
19.953	25.24	25.24	4.30	3.34	34.01	25.22	4.33	3.34	34.01	25.22	4.32	3.34	10^{-3}
25.119	12.62	12.62	1.91	1.49	17.11	12.55	1.90	1.50	17.13	12.60	1.91	1.49	10^{-3}
31.623	63.49	63.49	8.60	6.79	87.22	63.37	8.56	6.77	87.19	63.49	8.58	6.77	10^{-4}

TABLE III. Neutrino flux ($m^{-2}\,sec^{-1}\,sr^{-1}\,GeV^{-1}$) for $0.8 \geq \cos\theta_z > 0.7$.

	Kamioka				Sudbury				Gran Sasso				
E_ν (GeV)	ν_μ	$\bar{\nu}_\mu$	ν_e	$\bar{\nu}_e$	ν_μ	$\bar{\nu}_\mu$	ν_e	$\bar{\nu}_e$	ν_μ	$\bar{\nu}_\mu$	ν_e	$\bar{\nu}_e$	Norm
0.1000	4.46	4.46	2.12	2.17	12.68	12.82	6.38	5.70	7.74	7.84	3.75	3.70	10^3
0.1259	3.63	3.63	1.73	1.74	9.97	10.02	5.01	4.40	6.25	6.31	3.03	2.94	10^3
0.1585	2.88	2.88	1.36	1.35	7.50	7.51	3.77	3.24	4.88	4.90	2.35	2.24	10^3
0.1995	2.18	2.18	1.04	1.01	5.35	5.33	2.71	2.29	3.64	3.64	1.76	1.64	10^3
0.2512	15.92	15.92	7.63	7.30	36.02	35.91	18.63	15.42	25.92	25.74	12.63	11.50	10^2
0.3162	11.19	11.19	5.41	5.07	23.15	23.10	12.18	9.89	17.65	17.48	8.69	7.72	10^2
0.3981	7.60	7.60	3.68	3.40	14.28	14.19	7.57	6.06	11.59	11.41	5.72	4.98	10^2
0.5012	5.00	5.00	2.42	2.20	8.51	8.39	4.49	3.58	7.31	7.14	3.62	3.08	10^2
0.6310	3.18	3.18	1.54	1.37	4.92	4.82	2.58	2.04	4.46	4.31	2.20	1.84	10^2
0.7943	19.55	19.55	9.42	8.27	27.97	27.00	14.33	11.23	26.37	25.16	12.85	10.54	10^1
1.0000	11.76	11.76	5.62	4.81	15.64	14.88	7.74	6.06	15.18	14.31	7.25	5.83	10^1
1.2589	6.85	6.85	3.24	2.72	8.69	8.12	4.09	3.19	8.58	7.95	3.95	3.14	10^1
1.5849	3.90	3.90	1.80	1.48	4.81	4.36	2.13	1.66	4.77	4.33	2.10	1.64	10^1
1.9953	21.52	21.52	9.67	7.81	26.07	23.12	10.89	8.40	25.95	23.04	10.80	8.41	10^0
2.5119	11.62	11.62	5.03	3.98	13.91	12.09	5.41	4.19	13.92	12.11	5.41	4.18	10^0
3.1623	6.12	6.12	2.53	1.97	7.36	6.26	2.65	2.02	7.37	6.27	2.65	2.02	10^0
3.9811	31.87	31.87	12.36	9.49	38.67	32.12	12.65	9.61	38.57	32.19	12.67	9.62	10^{-1}
5.0119	16.31	16.31	5.85	4.49	20.02	16.39	5.95	4.49	20.04	16.41	5.99	4.51	10^{-1}
6.3096	8.30	8.30	2.73	2.08	10.35	8.33	2.74	2.07	10.36	8.31	2.75	2.09	10^{-1}
7.9433	41.98	41.98	12.58	9.60	53.19	42.10	12.53	9.40	53.22	41.93	12.40	9.43	10^{-2}
10.000	21.02	21.02	5.63	4.27	27.00	21.02	5.65	4.26	27.01	21.02	5.65	4.27	10^{-2}
12.589	10.54	10.54	2.51	1.91	13.72	10.54	2.51	1.92	13.72	10.54	2.52	1.92	10^{-2}
15.849	52.84	52.84	11.19	8.51	69.61	52.73	11.17	8.56	69.59	52.87	11.17	8.52	10^{-3}
19.953	26.43	26.43	4.91	3.80	35.20	26.35	4.91	3.81	35.18	26.41	4.92	3.80	10^{-3}
25.119	13.20	13.20	2.18	1.70	17.76	13.17	2.18	1.69	17.79	13.19	2.18	1.70	10^{-3}
31.623	66.54	66.54	9.75	7.67	90.68	66.58	9.78	7.69	90.69	66.55	9.75	7.69	10^{-4}

TABLE IV. Neutrino flux ($m^{-2}\,sec^{-1}\,sr^{-1}\,GeV^{-1}$) for $0.7 \geq \cos\theta_z > 0.6$.

	Kamioka				Sudbury				Gran Sasso				
E_ν (GeV)	ν_μ	$\bar{\nu}_\mu$	ν_e	$\bar{\nu}_e$	ν_μ	$\bar{\nu}_\mu$	ν_e	$\bar{\nu}_e$	ν_μ	$\bar{\nu}_\mu$	ν_e	$\bar{\nu}_e$	Norm
0.1000	4.63	4.63	2.20	2.24	13.31	13.43	6.67	5.99	8.05	8.17	3.90	3.85	10^3
0.1259	3.74	3.74	1.78	1.79	10.31	10.36	5.20	4.58	6.44	6.50	3.12	3.03	10^3
0.1585	2.94	2.94	1.40	1.38	7.70	7.70	3.88	3.35	4.98	5.02	2.41	2.29	10^3
0.1995	2.22	2.22	1.06	1.03	5.45	5.44	2.79	2.36	3.70	3.69	1.80	1.68	10^3
0.2512	16.09	16.09	7.82	7.43	36.61	36.53	19.16	15.84	26.20	26.11	12.95	11.77	10^2
0.3162	11.28	11.28	5.54	5.17	23.48	23.47	12.48	10.20	17.87	17.71	8.92	7.93	10^2
0.3981	7.69	7.69	3.79	3.49	14.51	14.45	7.80	6.28	11.73	11.55	5.89	5.15	10^2
0.5012	5.05	5.05	2.51	2.27	8.66	8.58	4.68	3.72	7.42	7.25	3.75	3.20	10^2
0.6310	3.22	3.22	1.61	1.42	5.03	4.93	2.70	2.13	4.54	4.39	2.29	1.92	10^2
0.7943	19.92	19.92	9.94	8.68	28.65	27.74	15.11	11.89	26.89	25.85	13.55	11.09	10^1
1.0000	12.01	12.01	5.97	5.08	16.10	15.38	8.24	6.46	15.57	14.77	7.72	6.22	10^1
1.2589	7.05	7.05	3.44	2.89	8.96	8.42	4.40	3.43	8.82	8.24	4.26	3.38	10^1
1.5849	4.02	4.02	1.93	1.59	4.95	4.55	2.31	1.79	4.92	4.51	2.27	1.78	10^1
1.9953	22.29	22.29	10.52	8.43	26.85	24.20	11.89	9.20	26.84	24.18	11.80	9.13	10^0
2.5119	12.07	12.07	5.52	4.37	14.36	12.70	6.00	4.60	14.34	12.66	5.96	4.58	10^0
3.1623	6.39	6.39	2.79	2.18	7.61	6.58	2.95	2.25	7.62	6.58	2.95	2.25	10^0
3.9811	3.33	3.33	1.38	1.06	3.98	3.38	1.42	1.08	3.99	3.38	1.42	1.08	10^0
5.0119	17.14	17.14	6.60	5.03	20.71	17.27	6.71	5.10	20.77	17.24	6.71	5.07	10^{-1}
6.3096	8.72	8.72	3.11	2.33	10.71	8.71	3.12	2.38	10.69	8.73	3.14	2.35	10^{-1}
7.9433	4.40	4.40	1.43	1.08	5.49	4.42	1.43	1.09	5.49	4.41	1.43	1.08	10^{-1}
10.000	22.13	22.13	6.49	4.90	27.97	22.12	6.49	4.91	27.96	22.10	6.48	4.90	10^{-2}
12.589	11.09	11.09	2.91	2.21	14.22	11.09	2.91	2.21	14.21	11.09	2.91	2.21	10^{-2}
15.849	55.59	55.59	12.94	9.83	72.17	55.62	12.98	9.88	72.11	55.59	12.92	9.86	10^{-3}
19.953	27.78	27.78	5.73	4.41	36.65	27.87	5.74	4.39	36.61	27.82	5.72	4.39	10^{-3}
25.119	13.91	13.91	2.54	1.96	18.50	13.92	2.53	1.97	18.49	13.90	2.52	1.95	10^{-3}
31.623	70.32	70.32	11.32	8.87	94.48	70.25	11.34	8.89	94.53	70.30	11.32	8.90	10^{-4}

TABLE V. Neutrino flux ($m^{-2}\,sec^{-1}\,sr^{-1}\,GeV^{-1}$) for $0.6 \geq \cos\theta_z > 0.5$.

	Kamioka				Sudbury				Gran Sasso				
E_ν (GeV)	ν_μ	$\bar{\nu}_\mu$	ν_e	$\bar{\nu}_e$	ν_μ	$\bar{\nu}_\mu$	ν_e	$\bar{\nu}_e$	ν_μ	$\bar{\nu}_\mu$	ν_e	$\bar{\nu}_e$	Norm
0.1000	4.88	4.88	2.31	2.35	14.19	14.33	7.11	6.38	8.53	8.65	4.11	4.06	10^3
0.1259	3.89	3.89	1.86	1.85	10.84	10.90	5.47	4.84	6.72	6.79	3.26	3.17	10^3
0.1585	3.03	3.03	1.45	1.42	8.00	8.00	4.05	3.50	5.15	5.17	2.50	2.37	10^3
0.1995	2.27	2.27	1.09	1.05	5.61	5.60	2.89	2.45	3.79	3.78	1.85	1.73	10^3
0.2512	16.35	16.35	8.02	7.58	37.43	37.37	19.71	16.38	26.66	26.53	13.28	12.09	10^2
0.3162	11.43	11.43	5.68	5.29	23.93	23.87	12.90	10.52	18.10	17.94	9.14	8.15	10^2
0.3981	7.77	7.77	3.90	3.56	14.77	14.72	8.08	6.52	11.87	11.69	6.06	5.30	10^2
0.5012	5.13	5.13	2.60	2.33	8.82	8.75	4.85	3.87	7.52	7.38	3.88	3.32	10^2
0.6310	3.27	3.27	1.67	1.48	5.14	5.06	2.83	2.24	4.62	4.49	2.39	2.00	10^2
0.7943	20.39	20.39	10.43	9.04	29.36	28.66	15.96	12.55	27.50	26.49	14.28	11.70	10^1
1.0000	12.31	12.31	6.30	5.37	16.54	15.94	8.80	6.90	15.96	15.25	8.19	6.61	10^1
1.2589	7.26	7.26	3.70	3.08	9.25	8.78	4.74	3.71	9.07	8.56	4.56	3.63	10^1
1.5849	4.16	4.16	2.09	1.72	5.13	4.76	2.52	1.96	5.08	4.72	2.46	1.94	10^1
1.9953	23.19	23.19	11.48	9.28	27.91	25.43	13.02	10.11	27.79	25.34	12.96	10.09	10^0
2.5119	12.64	12.64	6.09	4.80	14.93	13.38	6.65	5.12	14.93	13.40	6.65	5.11	10^0
3.1623	6.72	6.72	3.12	2.43	7.91	6.97	3.31	2.52	7.93	6.97	3.31	2.53	10^0
3.9811	3.52	3.52	1.55	1.20	4.15	3.58	1.61	1.22	4.16	3.59	1.61	1.22	10^0
5.0119	18.11	18.11	7.54	5.77	21.57	18.29	7.70	5.82	21.58	18.33	7.70	5.80	10^{-1}
6.3096	9.29	9.29	3.58	2.70	11.13	9.30	3.61	2.73	11.17	9.29	3.62	2.73	10^{-1}
7.9433	4.67	4.67	1.67	1.25	5.74	4.68	1.66	1.25	5.72	4.67	1.68	1.26	10^{-1}
10.000	23.45	23.45	7.60	5.72	29.11	23.47	7.61	5.72	29.08	23.45	7.61	5.72	10^{-2}
12.589	11.77	11.77	3.43	2.58	14.82	11.77	3.42	2.58	14.79	11.78	3.43	2.58	10^{-2}
15.849	5.89	5.89	1.53	1.16	7.53	5.90	1.53	1.16	7.53	5.90	1.53	1.16	10^{-2}
19.953	29.51	29.51	6.80	5.19	38.25	29.53	6.81	5.19	38.22	29.50	6.77	5.24	10^{-3}
25.119	14.75	14.75	3.00	2.33	19.35	14.79	3.02	2.31	19.33	14.78	3.03	2.32	10^{-3}
31.623	7.47	7.47	1.35	1.05	9.90	7.47	1.35	1.05	9.91	7.48	1.35	1.05	10^{-3}

TABLE VI. Neutrino flux ($m^{-2}\,sec^{-1}\,sr^{-1}\,GeV^{-1}$) for $0.5 \geq \cos\theta_z > 0.4$.

	Kamioka				Sudbury				Gran Sasso				
E_ν (GeV)	ν_μ	$\bar{\nu}_\mu$	ν_e	$\bar{\nu}_e$	ν_μ	$\bar{\nu}_\mu$	ν_e	$\bar{\nu}_e$	ν_μ	$\bar{\nu}_\mu$	ν_e	$\bar{\nu}_e$	Norm
0.1000	5.28	5.28	2.49	2.52	15.55	15.71	7.75	6.99	9.26	9.39	4.45	4.40	10^3
0.1259	4.15	4.15	1.97	1.97	11.65	11.72	5.89	5.22	7.18	7.25	3.48	3.39	10^3
0.1585	3.17	3.17	1.53	1.48	8.45	8.46	4.30	3.73	5.42	5.44	2.63	2.50	10^3
0.1995	2.35	2.35	1.14	1.09	5.86	5.84	3.03	2.57	3.93	3.92	1.93	1.80	10^3
0.2512	16.79	16.79	8.31	7.81	38.68	38.57	20.57	17.12	27.36	27.26	13.73	12.54	10^2
0.3162	11.64	11.64	5.86	5.41	24.52	24.50	13.39	10.96	18.40	18.27	9.41	8.39	10^2
0.3981	7.87	7.87	4.01	3.65	15.06	15.04	8.36	6.75	12.03	11.87	6.22	5.46	10^2
0.5012	5.17	5.17	2.68	2.39	9.02	8.94	5.04	4.05	7.62	7.47	3.99	3.42	10^2
0.6310	3.31	3.31	1.73	1.53	5.25	5.19	2.96	2.35	4.68	4.55	2.48	2.09	10^2
0.7943	20.67	20.67	10.91	9.47	30.11	29.49	16.85	13.31	27.92	27.09	14.86	12.31	10^1
1.0000	12.57	12.57	6.65	5.66	17.01	16.54	9.36	7.35	16.29	15.66	8.63	7.02	10^1
1.2589	7.44	7.44	3.93	3.28	9.57	9.15	5.11	4.00	9.34	8.89	4.87	3.90	10^1
1.5849	4.31	4.31	2.25	1.86	5.31	5.01	2.74	2.13	5.24	4.92	2.68	2.11	10^1
1.9953	2.43	2.43	1.25	1.01	2.91	2.69	1.44	1.13	2.89	2.67	1.43	1.11	10^1
2.5119	13.20	13.20	6.70	5.35	15.58	14.20	7.45	5.76	15.54	14.19	7.39	5.71	10^0
3.1623	7.09	7.09	3.51	2.73	8.28	7.41	3.74	2.87	8.29	7.42	3.74	2.85	10^0
3.9811	3.74	3.74	1.76	1.36	4.34	3.83	1.84	1.40	4.35	3.83	1.84	1.40	10^0
5.0119	19.32	19.32	8.68	6.61	22.62	19.58	8.93	6.69	22.58	19.58	8.90	6.73	10^{-1}
6.3096	9.86	9.86	4.17	3.17	11.65	9.97	4.21	3.17	11.67	10.00	4.24	3.19	10^{-1}
7.9433	5.01	5.01	1.97	1.48	5.99	5.02	1.97	1.48	6.00	5.01	1.98	1.48	10^{-1}
10.000	25.18	25.18	9.07	6.82	30.51	25.21	9.10	6.84	30.57	25.23	9.09	6.83	10^{-2}
12.589	12.64	12.64	4.13	3.11	15.53	12.62	4.12	3.11	15.55	12.65	4.13	3.12	10^{-2}
15.849	6.33	6.33	1.86	1.41	7.90	6.32	1.86	1.41	7.91	6.34	1.87	1.41	10^{-2}
19.953	31.70	31.70	8.36	6.34	40.21	31.73	8.33	6.34	40.25	31.76	8.33	6.35	10^{-3}
25.119	15.87	15.87	3.69	2.84	20.42	15.83	3.69	2.84	20.44	15.91	3.71	2.86	10^{-3}
31.623	8.04	8.04	1.66	1.28	10.45	8.04	1.67	1.28	10.47	8.05	1.66	1.29	10^{-3}

TABLE VII. Neutrino flux ($m^{-2}\,sec^{-1}\,sr^{-1}\,GeV^{-1}$) for $0.4 \geq \cos\theta_z > 0.3$.

	Kamioka				Sudbury				Gran Sasso				
E_ν (GeV)	ν_μ	$\bar{\nu}_\mu$	ν_e	$\bar{\nu}_e$	ν_μ	$\bar{\nu}_\mu$	ν_e	$\bar{\nu}_e$	ν_μ	$\bar{\nu}_\mu$	ν_e	$\bar{\nu}_e$	Norm
0.1000	5.93	5.93	2.78	2.80	17.73	17.92	8.82	7.96	10.45	10.62	4.99	4.95	10^3
0.1259	4.56	4.56	2.18	2.15	13.02	13.08	6.59	5.85	7.94	8.02	3.84	3.74	10^3
0.1585	3.44	3.44	1.65	1.60	9.26	9.27	4.72	4.11	5.88	5.91	2.86	2.73	10^3
0.1995	2.49	2.49	1.22	1.16	6.30	6.29	3.27	2.79	4.19	4.19	2.07	1.93	10^3
0.2512	17.56	17.56	8.77	8.18	40.80	40.89	21.94	18.33	28.67	28.53	14.48	13.24	10^2
0.3162	12.01	12.01	6.17	5.60	25.55	25.57	14.10	11.60	19.05	18.83	9.84	8.77	10^2
0.3981	8.06	8.06	4.19	3.74	15.57	15.52	8.72	7.08	12.29	12.12	6.47	5.64	10^2
0.5012	5.25	5.25	2.76	2.45	9.24	9.21	5.25	4.24	7.73	7.56	4.12	3.54	10^2
0.6310	3.36	3.36	1.78	1.56	5.39	5.32	3.08	2.46	4.72	4.61	2.54	2.16	10^2
0.7943	20.89	20.89	11.26	9.71	31.00	30.36	17.76	14.04	28.20	27.34	15.38	12.77	10^1
1.0000	12.75	12.75	6.95	5.89	17.53	17.12	9.92	7.85	16.53	15.95	9.03	7.36	10^1
1.2589	7.60	7.60	4.15	3.47	9.88	9.51	5.51	4.31	9.50	9.12	5.15	4.16	10^1
1.5849	4.45	4.45	2.40	1.98	5.52	5.23	2.98	2.34	5.41	5.11	2.86	2.29	10^1
1.9953	2.51	2.51	1.36	1.10	3.03	2.84	1.59	1.24	2.99	2.80	1.56	1.22	10^1
2.5119	13.88	13.88	7.44	5.95	16.36	15.18	8.34	6.46	16.23	15.00	8.25	6.39	10^0
3.1623	7.52	7.52	3.93	3.08	8.76	7.97	4.29	3.27	8.67	7.92	4.25	3.26	10^0
3.9811	4.00	4.00	2.03	1.57	4.59	4.15	2.14	1.63	4.58	4.13	2.13	1.61	10^0
5.0119	20.85	20.85	10.09	7.74	23.98	21.39	10.48	7.93	23.94	21.27	10.41	7.94	10^{-1}
6.3096	10.70	10.70	4.97	3.74	12.45	10.86	5.08	3.82	12.35	10.82	5.04	3.78	10^{-1}
7.9433	5.45	5.45	2.38	1.79	6.39	5.53	2.41	1.81	6.36	5.49	2.39	1.78	10^{-1}
10.000	27.50	27.50	11.12	8.36	32.45	27.55	11.17	8.37	32.41	27.50	11.14	8.36	10^{-2}
12.589	13.80	13.80	5.13	3.86	16.53	13.84	5.13	3.85	16.49	13.80	5.12	3.86	10^{-2}
15.849	6.91	6.91	2.34	1.76	8.43	6.93	2.34	1.76	8.41	6.91	2.34	1.76	10^{-2}
19.953	34.65	34.65	10.60	8.02	42.83	34.68	10.55	8.01	42.70	34.59	10.49	8.04	10^{-3}
25.119	17.35	17.35	4.72	3.60	21.72	17.40	4.75	3.64	21.73	17.37	4.73	3.62	10^{-3}
31.623	8.80	8.80	2.14	1.64	11.21	8.81	2.14	1.65	11.20	8.81	2.14	1.65	10^{-3}

TABLE VIII. Neutrino flux ($m^{-2}\,sec^{-1}\,sr^{-1}\,GeV^{-1}$) for $0.3 \geq \cos\theta_z > 0.2$.

	Kamioka				Sudbury				Gran Sasso				
E_ν (GeV)	ν_μ	$\bar{\nu}_\mu$	ν_e	$\bar{\nu}_e$	ν_μ	$\bar{\nu}_\mu$	ν_e	$\bar{\nu}_e$	ν_μ	$\bar{\nu}_\mu$	ν_e	$\bar{\nu}_e$	Norm
0.1000	7.15	7.15	3.32	3.36	21.70	21.92	10.74	9.74	12.65	12.85	6.00	5.98	10^3
0.1259	5.36	5.36	2.55	2.52	15.49	15.62	7.86	7.01	9.37	9.46	4.52	4.44	10^3
0.1585	3.95	3.95	1.90	1.83	10.79	10.79	5.51	4.81	6.79	6.81	3.30	3.15	10^3
0.1995	2.80	2.80	1.38	1.30	7.16	7.13	3.75	3.21	4.72	4.70	2.34	2.18	10^3
0.2512	19.25	19.25	9.74	8.95	45.31	45.26	24.59	20.55	31.50	31.30	16.08	14.67	10^2
0.3162	12.89	12.89	6.68	6.04	27.75	27.67	15.46	12.78	20.40	20.22	10.68	9.50	10^2
0.3981	8.48	8.48	4.47	3.93	16.56	16.50	9.42	7.69	12.91	12.70	6.87	6.02	10^2
0.5012	5.44	5.44	2.93	2.54	9.69	9.64	5.59	4.51	7.96	7.81	4.32	3.71	10^2
0.6310	3.44	3.44	1.89	1.61	5.60	5.51	3.25	2.62	4.81	4.70	2.66	2.24	10^2
0.7943	2.13	2.13	1.18	1.00	3.20	3.13	1.86	1.49	2.86	2.78	1.59	1.33	10^2
1.0000	12.99	12.99	7.25	6.09	18.10	17.74	10.47	8.34	16.77	16.17	9.33	7.68	10^1
1.2589	7.75	7.75	4.37	3.62	10.25	9.90	5.85	4.63	9.66	9.29	5.39	4.39	10^1
1.5849	4.56	4.56	2.57	2.10	5.73	5.48	3.23	2.53	5.51	5.25	3.03	2.44	10^1
1.9953	2.59	2.59	1.47	1.18	3.16	3.01	1.75	1.36	3.08	2.91	1.68	1.33	10^1
2.5119	14.54	14.54	8.20	6.54	17.12	16.13	9.34	7.23	16.89	15.84	9.06	7.14	10^0
3.1623	8.00	8.00	4.41	3.50	9.21	8.61	4.89	3.74	9.12	8.47	4.79	3.72	10^0
3.9811	4.29	4.29	2.34	1.82	4.88	4.51	2.50	1.90	4.84	4.46	2.47	1.88	10^0
5.0119	22.71	22.71	11.98	9.23	25.63	23.36	12.51	9.45	25.44	23.26	12.42	9.36	10^{-1}
6.3096	11.87	11.87	6.03	4.57	13.33	11.95	6.15	4.63	13.17	11.94	6.14	4.62	10^{-1}
7.9433	6.07	6.07	2.95	2.23	6.84	6.08	2.98	2.23	6.88	6.11	2.99	2.23	10^{-1}
10.000	3.07	3.07	1.41	1.06	3.50	3.08	1.41	1.06	3.50	3.08	1.41	1.06	10^{-1}
12.589	15.50	15.50	6.63	4.98	17.86	15.49	6.63	4.97	17.88	15.49	6.63	4.97	10^{-2}
15.849	7.78	7.78	3.08	2.32	9.12	7.78	3.07	2.30	9.12	7.78	3.08	2.32	10^{-2}
19.953	3.90	3.90	1.41	1.07	4.64	3.90	1.41	1.07	4.64	3.90	1.41	1.06	10^{-2}
25.119	19.54	19.54	6.41	4.88	23.66	19.52	6.39	4.90	23.61	19.54	6.40	4.88	10^{-3}
31.623	9.91	9.91	2.93	2.25	12.20	9.91	2.93	2.25	12.18	9.91	2.92	2.25	10^{-3}

TABLE IX. Neutrino flux ($m^{-2}\,sec^{-1}\,sr^{-1}\,GeV^{-1}$) for $0.2 \geq \cos\theta_z > 0.1$.

	Kamioka				Sudbury				Gran Sasso				
E_ν (GeV)	ν_μ	$\bar{\nu}_\mu$	ν_e	$\bar{\nu}_e$	ν_μ	$\bar{\nu}_\mu$	ν_e	$\bar{\nu}_e$	ν_μ	$\bar{\nu}_\mu$	ν_e	$\bar{\nu}_e$	Norm
0.1000	9.80	9.80	4.53	4.53	29.97	30.35	14.81	13.52	17.36	17.68	8.17	8.18	10^3
0.1259	7.14	7.14	3.39	3.32	20.86	20.98	10.57	9.47	12.52	12.61	6.02	5.92	10^3
0.1585	5.08	5.08	2.45	2.35	14.07	14.11	7.23	6.34	8.78	8.82	4.27	4.09	10^3
0.1995	3.51	3.51	1.73	1.62	9.06	9.04	4.78	4.09	5.92	5.92	2.95	2.75	10^3
0.2512	2.34	2.34	1.19	1.09	5.57	5.56	3.05	2.57	3.83	3.79	1.97	1.79	10^3
0.3162	15.13	15.13	7.94	7.04	32.95	32.93	18.66	15.46	23.90	23.76	12.75	11.32	10^2
0.3981	9.58	9.58	5.20	4.49	19.04	19.02	11.07	8.99	14.61	14.46	7.99	6.91	10^2
0.5012	6.03	6.03	3.31	2.82	10.85	10.77	6.35	5.15	8.75	8.64	4.86	4.14	10^2
0.6310	3.71	3.71	2.09	1.75	6.09	6.01	3.62	2.88	5.14	5.04	2.92	2.45	10^2
0.7943	2.25	2.25	1.28	1.06	3.40	3.34	2.02	1.62	3.00	2.93	1.72	1.42	10^2
1.0000	13.61	13.61	7.86	6.40	19.05	18.61	11.28	8.98	17.28	16.79	9.97	8.15	10^1
1.2589	8.08	8.08	4.67	3.77	10.68	10.32	6.28	4.95	9.96	9.55	5.68	4.61	10^1
1.5849	4.70	4.70	2.76	2.20	5.98	5.72	3.46	2.75	5.65	5.41	3.21	2.59	10^1
1.9953	2.70	2.70	1.58	1.27	3.31	3.15	1.92	1.50	3.17	3.00	1.79	1.44	10^1
2.5119	15.27	15.27	8.92	7.02	18.01	17.12	10.40	8.04	17.46	16.55	9.79	7.85	10^0
3.1623	8.47	8.47	4.94	3.88	9.78	9.24	5.55	4.25	9.53	8.99	5.32	4.17	10^0
3.9811	4.60	4.60	2.67	2.07	5.22	4.91	2.91	2.21	5.13	4.81	2.82	2.18	10^0
5.0119	2.49	2.49	1.42	1.08	2.74	2.59	1.49	1.13	2.73	2.55	1.46	1.12	10^0
6.3096	13.08	13.08	7.26	5.56	14.46	13.46	7.61	5.67	14.23	13.32	7.43	5.59	10^{-1}
7.9433	6.88	6.88	3.70	2.80	7.49	6.95	3.76	2.85	7.46	6.87	3.72	2.84	10^{-1}
10.000	3.49	3.49	1.82	1.37	3.85	3.52	1.84	1.38	3.84	3.51	1.84	1.38	10^{-1}
12.589	17.81	17.81	8.85	6.64	19.76	17.85	8.88	6.66	19.76	17.87	8.89	6.66	10^{-2}
15.849	9.03	9.03	4.22	3.18	10.12	9.03	4.24	3.19	10.12	9.04	4.23	3.17	10^{-2}
19.953	4.57	4.57	1.99	1.51	5.16	4.54	1.99	1.51	5.17	4.55	1.99	1.50	10^{-2}
25.119	22.88	22.88	9.32	7.08	26.26	22.87	9.24	7.05	26.41	22.86	9.30	7.04	10^{-3}
31.623	11.61	11.61	4.35	3.31	13.63	11.67	4.35	3.32	13.64	11.64	4.34	3.33	10^{-3}

TABLE X. Neutrino flux ($m^{-2}\,sec^{-1}\,sr^{-1}\,GeV^{-1}$) for $0.1 \geq \cos\theta_z > 0.0$.

	Kamioka				Sudbury				Gran Sasso				
E_ν (GeV)	ν_μ	$\bar{\nu}_\mu$	ν_e	$\bar{\nu}_e$	ν_μ	$\bar{\nu}_\mu$	ν_e	$\bar{\nu}_e$	ν_μ	$\bar{\nu}_\mu$	ν_e	$\bar{\nu}_e$	Norm
0.1000	15.94	15.94	7.20	7.32	48.03	48.70	23.42	21.70	28.03	28.57	13.04	13.14	10^3
0.1259	11.21	11.21	5.25	5.20	32.39	32.64	16.36	14.78	19.52	19.71	9.35	9.21	10^3
0.1585	7.70	7.70	3.68	3.53	21.19	21.31	10.82	9.64	13.23	13.31	6.45	6.20	10^3
0.1995	5.13	5.13	2.51	2.36	13.19	13.19	6.97	6.02	8.61	8.56	4.30	4.01	10^3
0.2512	3.27	3.27	1.67	1.51	7.79	7.81	4.31	3.63	5.34	5.31	2.78	2.51	10^3
0.3162	20.11	20.11	10.78	9.48	44.46	44.36	25.43	21.20	31.96	31.86	17.31	15.26	10^2
0.3981	12.30	12.30	6.84	5.74	24.66	24.57	14.53	11.85	18.69	18.51	10.44	8.96	10^2
0.5012	7.44	7.44	4.17	3.46	13.41	13.43	8.11	6.49	10.78	10.61	6.08	5.19	10^2
0.6310	4.40	4.40	2.53	2.08	7.26	7.15	4.38	3.55	6.08	5.92	3.57	2.93	10^2
0.7943	2.58	2.58	1.52	1.21	3.93	3.87	2.41	1.90	3.40	3.32	2.03	1.65	10^2
1.0000	15.17	15.17	9.00	7.10	21.25	20.81	12.85	10.23	19.06	18.64	11.33	9.18	10^1
1.2589	8.83	8.83	5.25	4.11	11.67	11.27	6.97	5.55	10.71	10.38	6.31	5.09	10^1
1.5849	5.10	5.10	3.08	2.37	6.41	6.17	3.77	2.99	5.98	5.76	3.52	2.78	10^1
1.9953	2.87	2.87	1.75	1.35	3.52	3.38	2.08	1.63	3.32	3.19	1.95	1.54	10^1
2.5119	16.18	16.18	9.73	7.49	19.03	18.31	11.29	8.83	18.47	17.45	10.66	8.43	10^0
3.1623	8.93	8.93	5.45	4.19	10.34	9.78	6.04	4.68	9.94	9.47	5.84	4.54	10^0
3.9811	4.91	4.91	2.96	2.27	5.51	5.22	3.22	2.47	5.41	5.13	3.07	2.43	10^0
5.0119	2.64	2.64	1.59	1.20	2.92	2.79	1.69	1.29	2.88	2.75	1.66	1.28	10^0
6.3096	14.26	14.26	8.31	6.35	15.35	14.48	8.83	6.62	15.38	14.55	8.73	6.69	10^{-1}
7.9433	7.47	7.47	4.34	3.36	8.09	7.65	4.48	3.43	8.07	7.64	4.56	3.47	10^{-1}
10.000	3.93	3.93	2.23	1.69	4.21	4.00	2.30	1.72	4.20	3.96	2.28	1.72	10^{-1}
12.589	20.27	20.27	11.34	8.50	21.81	20.55	11.52	8.66	21.82	20.49	11.50	8.67	10^{-2}
15.849	10.48	10.48	5.66	4.25	11.31	10.57	5.69	4.27	11.33	10.58	5.71	4.26	10^{-2}
19.953	5.39	5.39	2.78	2.08	5.83	5.36	2.78	2.11	5.83	5.40	2.79	2.11	10^{-2}
25.119	2.73	2.73	1.35	1.02	3.01	2.71	1.36	1.03	2.99	2.73	1.36	1.02	10^{-2}
31.623	14.02	14.02	6.52	4.98	15.65	14.08	6.54	5.01	15.62	14.06	6.57	5.02	10^{-3}

TABLE XI. Neutrino flux ($m^{-2}\,sec^{-1}\,sr^{-1}\,GeV^{-1}$) for $0.0 \geq \cos\theta_z > -0.1$.

	Kamioka				Sudbury				Gran Sasso				
E_ν (GeV)	ν_μ	$\bar{\nu}_\mu$	ν_e	$\bar{\nu}_e$	ν_μ	$\bar{\nu}_\mu$	ν_e	$\bar{\nu}_e$	ν_μ	$\bar{\nu}_\mu$	ν_e	$\bar{\nu}_e$	Norm
0.1000	17.11	17.11	7.76	7.86	46.20	46.96	22.44	20.95	28.33	28.90	13.36	13.18	10^3
0.1259	11.97	11.97	5.60	5.59	31.24	31.62	15.76	14.38	19.72	19.87	9.46	9.26	10^3
0.1585	8.18	8.18	3.92	3.78	20.60	20.68	10.48	9.40	13.29	13.37	6.53	6.18	10^3
0.1995	5.36	5.36	2.65	2.49	12.92	12.89	6.80	5.92	8.58	8.55	4.33	3.98	10^3
0.2512	3.38	3.38	1.73	1.59	7.68	7.67	4.21	3.59	5.30	5.28	2.78	2.50	10^3
0.3162	20.65	20.65	11.17	9.85	44.06	44.13	25.15	21.03	31.55	31.53	17.27	15.00	10^2
0.3981	12.58	12.58	6.95	5.91	24.66	24.54	14.53	11.81	18.31	18.35	10.35	8.81	10^2
0.5012	7.42	7.42	4.22	3.52	13.51	13.46	8.12	6.58	10.49	10.43	6.03	5.09	10^2
0.6310	4.40	4.40	2.54	2.06	7.38	7.28	4.44	3.57	5.97	5.85	3.49	2.87	10^2
0.7943	2.56	2.56	1.51	1.23	4.00	3.93	2.43	1.91	3.36	3.29	2.01	1.62	10^2
1.0000	14.96	14.96	8.92	7.05	21.50	21.15	13.02	10.39	18.83	18.40	11.17	9.00	10^1
1.2589	8.67	8.67	5.23	4.03	11.78	11.34	7.12	5.63	10.62	10.33	6.28	5.07	10^1
1.5849	5.04	5.04	3.02	2.38	6.50	6.22	3.83	3.04	5.90	5.76	3.51	2.77	10^1
1.9953	2.85	2.85	1.72	1.33	3.54	3.40	2.08	1.65	3.32	3.19	1.96	1.54	10^1
2.5119	16.06	16.06	9.56	7.44	19.25	18.41	11.19	8.91	18.41	17.46	10.75	8.42	10^0
3.1623	8.92	8.92	5.41	4.14	10.36	9.83	6.11	4.72	10.02	9.49	5.87	4.53	10^0
3.9811	4.87	4.87	2.91	2.27	5.51	5.27	3.23	2.47	5.43	5.15	3.10	2.41	10^0
5.0119	2.63	2.63	1.58	1.21	2.92	2.81	1.71	1.29	2.90	2.73	1.64	1.28	10^0
6.3096	14.00	14.00	8.33	6.36	15.43	14.55	8.88	6.64	15.31	14.45	8.69	6.58	10^{-1}
7.9433	7.49	7.49	4.35	3.41	8.12	7.63	4.52	3.44	8.12	7.66	4.45	3.41	10^{-1}
10.000	3.93	3.93	2.24	1.69	4.22	3.99	2.31	1.72	4.20	3.95	2.28	1.73	10^{-1}
12.589	20.29	20.29	11.34	8.48	21.88	20.55	11.57	8.62	21.84	20.51	11.49	8.67	10^{-2}
15.849	10.48	10.48	5.67	4.26	11.30	10.57	5.71	4.27	11.35	10.59	5.72	4.25	10^{-2}
19.953	5.40	5.40	2.78	2.08	5.82	5.38	2.78	2.11	5.83	5.39	2.80	2.12	10^{-2}
25.119	2.73	2.73	1.36	1.02	3.01	2.72	1.35	1.03	2.99	2.73	1.37	1.02	10^{-2}
31.623	14.03	14.03	6.50	4.97	15.66	14.05	6.55	5.00	15.60	14.09	6.58	5.01	10^{-3}

TABLE XII. Neutrino flux ($m^{-2}\,sec^{-1}\,sr^{-1}\,GeV^{-1}$) for $-0.1 \geq \cos\theta_z > -0.2$.

	Kamioka				Sudbury				Gran Sasso				
E_ν (GeV)	ν_μ	$\bar{\nu}_\mu$	ν_e	$\bar{\nu}_e$	ν_μ	$\bar{\nu}_\mu$	ν_e	$\bar{\nu}_e$	ν_μ	$\bar{\nu}_\mu$	ν_e	$\bar{\nu}_e$	Norm
0.1000	12.56	12.56	5.81	5.81	25.56	25.94	12.51	11.63	17.71	18.04	8.58	8.18	10^3
0.1259	8.94	8.94	4.27	4.18	17.98	18.12	9.03	8.25	12.60	12.72	6.26	5.84	10^3
0.1585	6.24	6.24	3.04	2.89	12.30	12.38	6.24	5.59	8.69	8.78	4.36	3.99	10^3
0.1995	4.18	4.18	2.09	1.94	8.07	8.06	4.20	3.67	5.77	5.80	2.97	2.65	10^3
0.2512	2.69	2.69	1.40	1.27	5.05	5.05	2.72	2.33	3.67	3.68	1.95	1.71	10^3
0.3162	16.89	16.89	9.05	8.03	30.64	30.52	17.09	14.31	22.59	22.71	12.46	10.64	10^2
0.3981	10.41	10.41	5.71	4.95	18.09	18.01	10.35	8.52	13.69	13.71	7.67	6.45	10^2
0.5012	6.32	6.32	3.53	3.02	10.47	10.39	6.08	4.98	8.16	8.13	4.61	3.86	10^2
0.6310	3.81	3.81	2.17	1.81	6.00	5.93	3.53	2.84	4.81	4.77	2.75	2.27	10^2
0.7943	2.27	2.27	1.31	1.09	3.41	3.35	2.01	1.61	2.81	2.76	1.63	1.32	10^2
1.0000	13.47	13.47	7.80	6.37	19.13	18.73	11.35	9.04	16.33	16.06	9.45	7.67	10^1
1.2589	7.93	7.93	4.62	3.75	10.76	10.47	6.34	5.03	9.47	9.19	5.44	4.40	10^1
1.5849	4.61	4.61	2.69	2.17	6.03	5.81	3.52	2.77	5.45	5.25	3.11	2.49	10^1
1.9953	2.66	2.66	1.54	1.25	3.34	3.19	1.93	1.50	3.08	2.95	1.75	1.40	10^1
2.5119	15.07	15.07	8.71	6.98	18.18	17.30	10.52	8.05	17.20	16.37	9.73	7.71	10^0
3.1623	8.36	8.36	4.86	3.83	9.79	9.28	5.55	4.26	9.45	8.93	5.28	4.11	10^0
3.9811	4.56	4.56	2.63	2.05	5.20	4.94	2.90	2.22	5.12	4.82	2.81	2.16	10^0
5.0119	2.45	2.45	1.39	1.08	2.75	2.57	1.49	1.13	2.73	2.56	1.46	1.12	10^0
6.3096	12.98	12.98	7.27	5.50	14.34	13.44	7.55	5.71	14.32	13.29	7.43	5.70	10^{-1}
7.9433	6.77	6.77	3.68	2.80	7.49	6.95	3.74	2.81	7.49	6.83	3.74	2.81	10^{-1}
10.000	3.49	3.49	1.81	1.36	3.84	3.52	1.84	1.37	3.84	3.52	1.84	1.37	10^{-1}
12.589	17.79	17.79	8.85	6.63	19.74	17.84	8.91	6.64	19.76	17.86	8.89	6.65	10^{-2}
15.849	9.01	9.01	4.23	3.18	10.12	9.01	4.23	3.19	10.11	9.03	4.23	3.18	10^{-2}
19.953	4.54	4.54	2.00	1.50	5.17	4.54	2.00	1.51	5.17	4.56	2.00	1.51	10^{-2}
25.119	22.74	22.74	9.23	7.02	26.41	22.79	9.24	7.02	26.50	22.84	9.36	7.06	10^{-3}
31.623	11.60	11.60	4.35	3.30	13.65	11.65	4.35	3.31	13.64	11.62	4.34	3.31	10^{-3}

TABLE XIII. Neutrino flux ($m^{-2}\,sec^{-1}\,sr^{-1}\,GeV^{-1}$) for $-0.2 \geq \cos\theta_z > -0.3$.

	Kamioka				Sudbury				Gran Sasso				
E_ν (GeV)	ν_μ	$\bar{\nu}_\mu$	ν_e	$\bar{\nu}_e$	ν_μ	$\bar{\nu}_\mu$	ν_e	$\bar{\nu}_e$	ν_μ	$\bar{\nu}_\mu$	ν_e	$\bar{\nu}_e$	Norm
0.1000	10.41	10.41	4.95	4.75	15.38	15.62	7.58	7.05	12.45	12.68	6.14	5.71	10^3
0.1259	7.55	7.55	3.68	3.48	11.19	11.33	5.63	5.15	9.07	9.19	4.55	4.16	10^3
0.1585	5.34	5.34	2.64	2.44	7.93	8.00	4.01	3.60	6.44	6.49	3.26	2.93	10^3
0.1995	3.65	3.65	1.85	1.67	5.40	5.42	2.79	2.45	4.39	4.41	2.26	2.00	10^3
0.2512	2.39	2.39	1.25	1.11	3.53	3.54	1.88	1.62	2.88	2.89	1.53	1.33	10^3
0.3162	15.27	15.27	8.20	7.15	22.38	22.41	12.23	10.35	18.31	18.37	9.97	8.50	10^2
0.3981	9.62	9.62	5.24	4.51	13.84	13.86	7.69	6.45	11.41	11.40	6.32	5.27	10^2
0.5012	5.91	5.91	3.29	2.77	8.41	8.37	4.75	3.93	6.97	6.95	3.94	3.25	10^2
0.6310	3.61	3.61	2.02	1.71	5.03	4.97	2.86	2.33	4.22	4.19	2.38	1.96	10^2
0.7943	2.17	2.17	1.23	1.03	2.95	2.91	1.69	1.37	2.51	2.49	1.43	1.16	10^2
1.0000	12.97	12.97	7.36	6.06	17.18	16.80	9.83	7.90	14.88	14.61	8.39	6.83	10^1
1.2589	7.66	7.66	4.32	3.56	9.88	9.62	5.63	4.47	8.74	8.48	4.89	3.94	10^1
1.5849	4.44	4.44	2.52	2.06	5.61	5.40	3.15	2.49	5.05	4.86	2.79	2.23	10^1
1.9953	2.55	2.55	1.43	1.16	3.14	2.98	1.74	1.35	2.87	2.73	1.56	1.25	10^1
2.5119	14.24	14.24	8.02	6.41	17.07	16.10	9.31	7.22	15.91	15.06	8.62	6.72	10^0
3.1623	7.84	7.84	4.33	3.43	9.19	8.56	4.87	3.74	8.78	8.21	4.61	3.56	10^0
3.9811	4.23	4.23	2.29	1.78	4.88	4.51	2.49	1.90	4.72	4.37	2.39	1.83	10^0
5.0119	22.47	22.47	11.85	9.07	25.44	23.28	12.54	9.47	25.07	23.04	12.25	9.26	10^{-1}
6.3096	11.69	11.69	5.95	4.55	13.25	12.01	6.17	4.63	13.18	11.89	6.10	4.56	10^{-1}
7.9433	6.05	6.05	2.91	2.22	6.89	6.12	2.97	2.25	6.79	6.06	2.97	2.21	10^{-1}
10.000	3.06	3.06	1.40	1.05	3.50	3.08	1.42	1.06	3.49	3.07	1.41	1.06	10^{-1}
12.589	15.44	15.44	6.61	4.96	17.88	15.50	6.63	4.96	17.86	15.44	6.64	4.97	10^{-2}
15.849	7.75	7.75	3.07	2.31	9.11	7.77	3.07	2.31	9.12	7.77	3.08	2.31	10^{-2}
19.953	3.89	3.89	1.40	1.06	4.65	3.90	1.41	1.07	4.65	3.89	1.41	1.06	10^{-2}
25.119	19.46	19.46	6.38	4.86	23.63	19.52	6.43	4.87	23.65	19.54	6.39	4.87	10^{-3}
31.623	9.90	9.90	2.93	2.23	12.17	9.90	2.92	2.24	12.16	9.88	2.92	2.23	10^{-3}

TABLE XIV. Neutrino flux ($m^{-2}\,sec^{-1}\,sr^{-1}\,GeV^{-1}$) for $-0.3 \geq \cos\theta_z > -0.4$.

	Kamioka				Sudbury				Gran Sasso				
E_ν (GeV)	ν_μ	$\bar{\nu}_\mu$	ν_e	$\bar{\nu}_e$	ν_μ	$\bar{\nu}_\mu$	ν_e	$\bar{\nu}_e$	ν_μ	$\bar{\nu}_\mu$	ν_e	$\bar{\nu}_e$	Norm
0.1000	8.80	8.80	4.26	4.01	10.71	10.89	5.29	4.91	9.89	10.05	4.89	4.54	10^3
0.1259	6.53	6.53	3.21	2.99	7.99	8.08	4.00	3.67	7.37	7.47	3.70	3.38	10^3
0.1585	4.72	4.72	2.35	2.15	5.82	5.87	2.93	2.65	5.37	5.41	2.71	2.42	10^3
0.1995	3.29	3.29	1.67	1.50	4.08	4.09	2.09	1.84	3.74	3.76	1.92	1.69	10^3
0.2512	2.21	2.21	1.15	1.01	2.74	2.74	1.44	1.25	2.51	2.52	1.32	1.14	10^3
0.3162	14.38	14.38	7.64	6.66	17.81	17.86	9.55	8.18	16.28	16.34	8.74	7.47	10^2
0.3981	9.20	9.20	4.96	4.26	11.36	11.34	6.18	5.21	10.35	10.38	5.63	4.76	10^2
0.5012	5.71	5.71	3.12	2.67	7.06	7.01	3.88	3.26	6.45	6.42	3.54	2.95	10^2
0.6310	3.51	3.51	1.94	1.64	4.31	4.26	2.38	1.97	3.94	3.89	2.17	1.79	10^2
0.7943	21.25	21.25	11.80	9.91	25.88	25.41	14.29	11.79	23.73	23.29	13.07	10.76	10^1
1.0000	12.66	12.66	7.02	5.86	15.32	14.90	8.40	6.85	14.09	13.75	7.69	6.30	10^1
1.2589	7.45	7.45	4.10	3.41	8.92	8.62	4.84	3.90	8.24	7.96	4.45	3.61	10^1
1.5849	4.30	4.30	2.35	1.92	5.13	4.88	2.71	2.17	4.78	4.55	2.50	2.02	10^1
1.9953	2.44	2.44	1.32	1.07	2.88	2.71	1.49	1.17	2.71	2.55	1.39	1.11	10^1
2.5119	13.52	13.52	7.25	5.76	15.82	14.68	7.99	6.21	15.03	13.97	7.52	5.94	10^0
3.1623	7.35	7.35	3.84	3.01	8.55	7.80	4.16	3.20	8.23	7.54	3.96	3.09	10^0
3.9811	3.93	3.93	1.98	1.54	4.54	4.09	2.10	1.60	4.44	4.00	2.02	1.56	10^0
5.0119	20.58	20.58	9.94	7.67	23.76	21.14	10.41	7.89	23.47	20.89	10.16	7.74	10^{-1}
6.3096	10.65	10.65	4.91	3.75	12.31	10.78	5.07	3.78	12.22	10.73	4.98	3.75	10^{-1}
7.9433	5.44	5.44	2.34	1.76	6.37	5.46	2.40	1.79	6.34	5.47	2.38	1.80	10^{-1}
10.000	27.41	27.41	11.06	8.31	32.42	27.52	11.16	8.35	32.33	27.47	11.11	8.34	10^{-2}
12.589	13.79	13.79	5.12	3.85	16.52	13.78	5.13	3.86	16.50	13.80	5.14	3.85	10^{-2}
15.849	6.91	6.91	2.33	1.76	8.41	6.93	2.34	1.76	8.41	6.93	2.34	1.77	10^{-2}
19.953	34.66	34.66	10.55	8.03	42.75	34.56	10.53	7.98	42.78	34.69	10.55	8.01	10^{-3}
25.119	17.34	17.34	4.74	3.62	21.71	17.35	4.72	3.64	21.75	17.33	4.73	3.62	10^{-3}
31.623	8.78	8.78	2.13	1.64	11.18	8.79	2.14	1.65	11.18	8.80	2.14	1.65	10^{-3}

TABLE XV. Neutrino flux ($m^{-2}\,sec^{-1}\,sr^{-1}\,GeV^{-1}$) for $-0.4 \geq \cos\theta_z > -0.5$.

	Kamioka				Sudbury				Gran Sasso				
E_ν (GeV)	ν_μ	$\bar{\nu}_\mu$	ν_e	$\bar{\nu}_e$	ν_μ	$\bar{\nu}_\mu$	ν_e	$\bar{\nu}_e$	ν_μ	$\bar{\nu}_\mu$	ν_e	$\bar{\nu}_e$	Norm
0.1000	7.89	7.89	3.83	3.61	8.34	8.46	4.11	3.86	8.52	8.64	4.22	3.92	10^3
0.1259	6.00	6.00	2.95	2.75	6.38	6.45	3.18	2.94	6.50	6.57	3.25	2.98	10^3
0.1585	4.43	4.43	2.20	2.01	4.74	4.77	2.37	2.16	4.82	4.86	2.42	2.18	10^3
0.1995	3.14	3.14	1.59	1.43	3.39	3.39	1.71	1.53	3.44	3.45	1.75	1.55	10^3
0.2512	21.51	21.51	11.07	9.81	23.24	23.29	12.01	10.54	23.42	23.48	12.15	10.60	10^2
0.3162	14.25	14.25	7.46	6.55	15.41	15.38	8.10	7.02	15.45	15.45	8.17	7.01	10^2
0.3981	9.19	9.19	4.89	4.23	9.97	9.92	5.30	4.54	9.96	9.91	5.32	4.51	10^2
0.5012	5.79	5.79	3.11	2.67	6.30	6.25	3.36	2.86	6.25	6.21	3.35	2.83	10^2
0.6310	3.56	3.56	1.92	1.64	3.88	3.83	2.08	1.74	3.85	3.78	2.06	1.72	10^2
0.7943	21.45	21.45	11.62	9.82	23.59	22.98	12.53	10.42	23.19	22.62	12.34	10.22	10^1
1.0000	12.75	12.75	6.87	5.75	14.05	13.57	7.37	6.07	13.75	13.26	7.22	5.95	10^1
1.2589	7.44	7.44	3.97	3.29	8.24	7.87	4.22	3.46	8.04	7.68	4.14	3.38	10^1
1.5849	4.25	4.25	2.24	1.83	4.75	4.47	2.37	1.91	4.64	4.36	2.32	1.87	10^1
1.9953	23.82	23.82	12.40	9.95	26.75	24.83	12.98	10.40	26.11	24.26	12.58	10.08	10^0
2.5119	13.03	13.03	6.59	5.29	14.75	13.48	6.92	5.44	14.40	13.17	6.74	5.30	10^0
3.1623	6.99	6.99	3.43	2.69	8.01	7.17	3.56	2.76	7.84	7.05	3.47	2.71	10^0
3.9811	3.68	3.68	1.74	1.35	4.26	3.76	1.79	1.37	4.20	3.70	1.76	1.35	10^0
5.0119	19.20	19.20	8.58	6.58	22.34	19.42	8.74	6.64	22.13	19.24	8.62	6.59	10^{-1}
6.3096	9.82	9.82	4.13	3.15	11.61	9.91	4.19	3.15	11.56	9.87	4.15	3.15	10^{-1}
7.9433	5.03	5.03	1.96	1.47	5.97	5.03	1.99	1.47	5.95	5.00	1.96	1.48	10^{-1}
10.000	25.16	25.16	9.06	6.81	30.53	25.21	9.08	6.82	30.47	25.16	9.06	6.82	10^{-2}
12.589	12.65	12.65	4.13	3.11	15.53	12.64	4.14	3.11	15.53	12.64	4.13	3.11	10^{-2}
15.849	6.33	6.33	1.86	1.41	7.92	6.34	1.86	1.41	7.90	6.33	1.86	1.41	10^{-2}
19.953	31.71	31.71	8.32	6.33	40.20	31.70	8.33	6.32	40.29	31.71	8.34	6.34	10^{-3}
25.119	15.85	15.85	3.68	2.85	20.45	15.90	3.70	2.86	20.44	15.91	3.70	2.83	10^{-3}
31.623	8.04	8.04	1.66	1.28	10.47	8.05	1.66	1.29	10.47	8.05	1.66	1.29	10^{-3}

TABLE XVI. Neutrino flux ($m^{-2}\,sec^{-1}\,sr^{-1}\,GeV^{-1}$) for $-0.5 \geq \cos\theta_z > -0.6$.

	Kamioka				Sudbury				Gran Sasso				
E_ν (GeV)	ν_μ	$\bar{\nu}_\mu$	ν_e	$\bar{\nu}_e$	ν_μ	$\bar{\nu}_\mu$	ν_e	$\bar{\nu}_e$	ν_μ	$\bar{\nu}_\mu$	ν_e	$\bar{\nu}_e$	Norm
0.1000	7.89	7.89	3.83	3.62	6.84	6.93	3.35	3.20	7.88	7.99	3.90	3.66	10^3
0.1259	6.10	6.10	2.99	2.80	5.35	5.40	2.64	2.48	6.13	6.21	3.05	2.83	10^3
0.1585	4.59	4.59	2.26	2.08	4.06	4.08	2.00	1.86	4.65	4.68	2.32	2.11	10^3
0.1995	3.31	3.31	1.65	1.49	2.96	2.95	1.47	1.34	3.36	3.37	1.69	1.51	10^3
0.2512	2.28	2.28	1.16	1.03	2.07	2.06	1.04	0.93	2.34	2.33	1.19	1.05	10^3
0.3162	15.22	15.22	7.91	6.90	13.95	13.85	7.13	6.31	15.61	15.58	8.10	7.00	10^2
0.3981	9.84	9.84	5.16	4.46	9.15	9.07	4.72	4.11	10.11	10.03	5.29	4.52	10^2
0.5012	6.18	6.18	3.26	2.80	5.84	5.75	3.01	2.60	6.38	6.29	3.34	2.82	10^2
0.6310	3.77	3.77	2.00	1.69	3.64	3.56	1.87	1.60	3.92	3.84	2.06	1.71	10^2
0.7943	2.25	2.25	1.20	1.00	2.22	2.15	1.13	0.96	2.35	2.28	1.22	1.00	10^2
1.0000	13.18	13.18	6.95	5.75	13.31	12.77	6.67	5.55	13.85	13.29	7.04	5.77	10^1
1.2589	7.56	7.56	3.94	3.21	7.84	7.40	3.81	3.14	8.05	7.62	3.98	3.23	10^1
1.5849	4.26	4.26	2.17	1.76	4.53	4.21	2.13	1.73	4.59	4.26	2.19	1.76	10^1
1.9953	23.41	23.41	11.66	9.35	25.52	23.31	11.58	9.27	25.58	23.46	11.71	9.35	10^0
2.5119	12.69	12.69	6.13	4.81	14.07	12.65	6.12	4.83	14.07	12.63	6.12	4.81	10^0
3.1623	6.70	6.70	3.13	2.43	7.64	6.73	3.13	2.43	7.59	6.69	3.11	2.42	10^0
3.9811	3.50	3.50	1.55	1.19	4.07	3.52	1.56	1.19	4.03	3.49	1.54	1.19	10^0
5.0119	18.08	18.08	7.51	5.71	21.42	18.17	7.55	5.77	21.22	18.04	7.51	5.71	10^{-1}
6.3096	9.27	9.27	3.58	2.70	11.10	9.27	3.60	2.71	11.06	9.21	3.57	2.67	10^{-1}
7.9433	4.70	4.70	1.66	1.25	5.74	4.68	1.66	1.26	5.68	4.65	1.65	1.26	10^{-1}
10.000	23.43	23.43	7.59	5.72	29.08	23.45	7.59	5.72	29.05	23.44	7.58	5.71	10^{-2}
12.589	11.77	11.77	3.43	2.58	14.80	11.76	3.42	2.58	14.80	11.74	3.43	2.59	10^{-2}
15.849	5.89	5.89	1.53	1.16	7.51	5.88	1.53	1.16	7.51	5.89	1.53	1.16	10^{-2}
19.953	29.49	29.49	6.75	5.23	38.14	29.47	6.77	5.19	38.13	29.48	6.78	5.20	10^{-3}
25.119	14.75	14.75	3.00	2.32	19.31	14.73	3.01	2.33	19.38	14.75	3.02	2.33	10^{-3}
31.623	7.48	7.48	1.35	1.05	9.91	7.47	1.35	1.05	9.90	7.47	1.35	1.05	10^{-3}

TABLE XVII. Neutrino flux ($m^{-2}\,sec^{-1}\,sr^{-1}\,GeV^{-1}$) for $-0.6 \geq \cos\theta_z > -0.7$.

	Kamioka				Sudbury				Gran Sasso				
E_ν (GeV)	ν_μ	$\bar{\nu}_\mu$	ν_e	$\bar{\nu}_e$	ν_μ	$\bar{\nu}_\mu$	ν_e	$\bar{\nu}_e$	ν_μ	$\bar{\nu}_\mu$	ν_e	$\bar{\nu}_e$	Norm
0.1000	8.31	8.31	4.07	3.82	5.63	5.71	2.73	2.70	7.40	7.53	3.64	3.49	10^3
0.1259	6.52	6.52	3.20	2.97	4.52	4.55	2.19	2.14	5.89	5.96	2.90	2.74	10^3
0.1585	4.94	4.94	2.44	2.21	3.52	3.52	1.70	1.63	4.54	4.56	2.23	2.06	10^3
0.1995	3.57	3.57	1.78	1.59	2.62	2.61	1.27	1.20	3.33	3.34	1.65	1.50	10^3
0.2512	2.47	2.47	1.26	1.10	1.88	1.86	0.92	0.85	2.34	2.34	1.17	1.04	10^3
0.3162	16.41	16.41	8.46	7.30	12.96	12.82	6.38	5.82	15.81	15.72	8.02	7.02	10^2
0.3981	10.52	10.52	5.48	4.66	8.64	8.50	4.27	3.83	10.31	10.19	5.26	4.53	10^2
0.5012	6.53	6.53	3.42	2.88	5.60	5.48	2.77	2.45	6.49	6.38	3.32	2.81	10^2
0.6310	3.92	3.92	2.06	1.72	3.54	3.42	1.74	1.51	3.97	3.86	2.02	1.69	10^2
0.7943	23.09	23.09	12.12	9.98	21.66	20.84	10.53	9.03	23.68	22.83	11.89	9.81	10^1
1.0000	13.33	13.33	6.89	5.60	13.03	12.37	6.22	5.22	13.84	13.17	6.80	5.56	10^1
1.2589	7.54	7.54	3.82	3.08	7.66	7.17	3.53	2.95	7.96	7.47	3.77	3.05	10^1
1.5849	4.20	4.20	2.07	1.65	4.41	4.06	1.97	1.60	4.51	4.16	2.05	1.64	10^1
1.9953	22.84	22.84	10.96	8.64	24.81	22.44	10.59	8.49	25.09	22.67	10.83	8.57	10^0
2.5119	12.25	12.25	5.63	4.42	13.67	12.10	5.53	4.35	13.70	12.10	5.59	4.37	10^0
3.1623	6.43	6.43	2.83	2.19	7.37	6.40	2.82	2.18	7.35	6.38	2.81	2.18	10^0
3.9811	3.34	3.34	1.38	1.06	3.93	3.33	1.38	1.06	3.91	3.31	1.37	1.05	10^0
5.0119	17.14	17.14	6.63	5.05	20.56	17.16	6.63	5.03	20.41	17.02	6.59	5.03	10^{-1}
6.3096	8.74	8.74	3.12	2.35	10.68	8.72	3.12	2.37	10.67	8.69	3.10	2.35	10^{-1}
7.9433	4.42	4.42	1.44	1.09	5.48	4.42	1.44	1.08	5.46	4.41	1.42	1.07	10^{-1}
10.000	22.12	22.12	6.48	4.90	27.95	22.12	6.49	4.90	27.94	22.10	6.47	4.90	10^{-2}
12.589	11.08	11.08	2.91	2.20	14.22	11.09	2.91	2.20	14.20	11.09	2.91	2.21	10^{-2}
15.849	55.62	55.62	12.92	9.90	72.17	55.51	12.93	9.88	72.17	55.50	12.93	9.81	10^{-3}
19.953	27.76	27.76	5.73	4.39	36.55	27.81	5.73	4.39	36.56	27.87	5.74	4.40	10^{-3}
25.119	13.89	13.89	2.53	1.96	18.48	13.91	2.53	1.96	18.51	13.95	2.55	1.96	10^{-3}
31.623	70.11	70.11	11.34	8.86	94.53	70.21	11.32	8.87	94.39	70.16	11.34	8.90	10^{-4}

TABLE XVIII. Neutrino flux ($m^{-2}\,sec^{-1}\,sr^{-1}\,GeV^{-1}$) for $-0.7 \geq \cos\theta_z > -0.8$.

	Kamioka				Sudbury				Gran Sasso				
E_ν (GeV)	ν_μ	$\bar{\nu}_\mu$	ν_e	$\bar{\nu}_e$	ν_μ	$\bar{\nu}_\mu$	ν_e	$\bar{\nu}_e$	ν_μ	$\bar{\nu}_\mu$	ν_e	$\bar{\nu}_e$	Norm
0.1000	7.96	7.96	3.89	3.65	5.33	5.39	2.57	2.58	6.59	6.69	3.24	3.11	10^3
0.1259	6.32	6.32	3.11	2.87	4.33	4.36	2.08	2.06	5.31	5.36	2.60	2.47	10^3
0.1585	4.84	4.84	2.37	2.16	3.41	3.41	1.63	1.58	4.13	4.15	2.01	1.88	10^3
0.1995	3.53	3.53	1.75	1.56	2.57	2.56	1.23	1.17	3.07	3.08	1.50	1.37	10^3
0.2512	2.45	2.45	1.23	1.08	1.86	1.84	0.89	0.83	2.17	2.17	1.07	0.96	10^3
0.3162	16.33	16.33	8.29	7.17	12.92	12.73	6.23	5.71	14.78	14.68	7.34	6.49	10^2
0.3981	10.48	10.48	5.36	4.57	8.65	8.50	4.19	3.77	9.71	9.56	4.82	4.19	10^2
0.5012	6.48	6.48	3.32	2.79	5.62	5.49	2.71	2.39	6.14	6.03	3.05	2.60	10^2
0.6310	3.88	3.88	2.00	1.66	3.53	3.41	1.69	1.46	3.78	3.67	1.86	1.57	10^2
0.7943	22.80	22.80	11.62	9.51	21.61	20.64	10.14	8.67	22.70	21.80	10.95	9.12	10^1
1.0000	13.08	13.08	6.54	5.33	12.88	12.16	5.94	4.97	13.34	12.62	6.27	5.14	10^1
1.2589	7.38	7.38	3.61	2.91	7.55	7.00	3.36	2.77	7.71	7.17	3.49	2.83	10^1
1.5849	4.08	4.08	1.94	1.54	4.32	3.93	1.85	1.50	4.39	4.00	1.89	1.51	10^1
1.9953	22.17	22.17	10.17	7.99	24.30	21.64	9.82	7.82	24.35	21.75	9.92	7.89	10^0
2.5119	11.75	11.75	5.18	4.03	13.32	11.63	5.05	3.98	13.29	11.64	5.11	3.98	10^0
3.1623	6.16	6.16	2.57	1.98	7.16	6.12	2.53	1.97	7.14	6.11	2.53	1.96	10^0
3.9811	31.88	31.88	12.42	9.52	37.98	31.74	12.33	9.47	37.93	31.68	12.31	9.49	10^{-1}
5.0119	16.36	16.36	5.88	4.46	19.90	16.32	5.86	4.47	19.88	16.30	5.83	4.46	10^{-1}
6.3096	8.31	8.31	2.74	2.08	10.32	8.29	2.74	2.07	10.29	8.28	2.72	2.06	10^{-1}
7.9433	41.84	41.84	12.58	9.48	53.00	41.93	12.40	9.48	53.01	41.86	12.52	9.47	10^{-2}
10.000	21.01	21.01	5.64	4.27	26.96	21.03	5.64	4.27	26.98	21.00	5.64	4.27	10^{-2}
12.589	10.53	10.53	2.51	1.92	13.70	10.53	2.51	1.91	13.70	10.53	2.51	1.92	10^{-2}
15.849	52.76	52.76	11.18	8.54	69.47	52.74	11.16	8.53	69.56	52.79	11.20	8.54	10^{-3}
19.953	26.41	26.41	4.92	3.82	35.19	26.41	4.92	3.80	35.27	26.40	4.92	3.79	10^{-3}
25.119	13.20	13.20	2.18	1.69	17.73	13.16	2.18	1.69	17.77	13.20	2.18	1.69	10^{-3}
31.623	66.52	66.52	9.75	7.70	90.59	66.56	9.79	7.64	90.64	66.58	9.78	7.68	10^{-4}

TABLE XIX. Neutrino flux ($m^{-2}\,sec^{-1}\,sr^{-1}\,GeV^{-1}$) for $-0.8 \geq \cos\theta_z > -0.9$.

	Kamioka				Sudbury				Gran Sasso				
E_ν (GeV)	ν_μ	$\bar{\nu}_\mu$	ν_e	$\bar{\nu}_e$	ν_μ	$\bar{\nu}_\mu$	ν_e	$\bar{\nu}_e$	ν_μ	$\bar{\nu}_\mu$	ν_e	$\bar{\nu}_e$	Norm
0.1000	7.04	7.04	3.45	3.25	6.42	6.46	3.15	3.01	6.37	6.43	3.15	2.97	10^3
0.1259	5.67	5.67	2.78	2.57	5.18	5.20	2.53	2.38	5.15	5.19	2.53	2.36	10^3
0.1585	4.39	4.39	2.13	1.95	4.03	4.02	1.95	1.80	4.01	4.02	1.95	1.79	10^3
0.1995	3.23	3.23	1.58	1.42	2.98	2.96	1.44	1.31	2.97	2.96	1.45	1.30	10^3
0.2512	22.57	22.57	11.16	9.84	20.94	20.78	10.22	9.13	20.92	20.79	10.26	9.11	10^2
0.3162	15.12	15.12	7.54	6.57	14.12	13.96	6.91	6.07	14.12	13.99	6.95	6.08	10^2
0.3981	9.77	9.77	4.87	4.19	9.18	9.02	4.49	3.89	9.22	9.10	4.50	3.90	10^2
0.5012	6.09	6.09	3.03	2.59	5.79	5.65	2.80	2.40	5.82	5.69	2.83	2.42	10^2
0.6310	3.68	3.68	1.83	1.53	3.54	3.42	1.70	1.43	3.58	3.46	1.71	1.44	10^2
0.7943	21.70	21.70	10.70	8.82	21.24	20.30	9.90	8.28	21.53	20.54	10.01	8.35	10^1
1.0000	12.51	12.51	6.02	4.94	12.52	11.79	5.62	4.65	12.70	11.95	5.70	4.72	10^1
1.2589	7.08	7.08	3.31	2.69	7.29	6.72	3.11	2.55	7.39	6.83	3.16	2.58	10^1
1.5849	3.92	3.92	1.78	1.43	4.17	3.76	1.69	1.36	4.22	3.82	1.71	1.38	10^1
1.9953	21.24	21.24	9.34	7.34	23.30	20.58	8.88	7.09	23.55	20.75	9.00	7.16	10^0
2.5119	11.27	11.27	4.73	3.70	12.78	11.05	4.55	3.59	12.85	11.12	4.60	3.62	10^0
3.1623	5.92	5.92	2.33	1.80	6.91	5.83	2.27	1.77	6.94	5.84	2.30	1.78	10^0
3.9811	30.52	30.52	11.25	8.57	36.69	30.32	11.05	8.49	36.81	30.32	11.08	8.50	10^{-1}
5.0119	15.67	15.67	5.29	4.02	19.28	15.60	5.23	4.00	19.28	15.59	5.24	3.99	10^{-1}
6.3096	7.96	7.96	2.43	1.86	9.99	7.93	2.42	1.84	10.03	7.91	2.43	1.84	10^{-1}
7.9433	40.17	40.17	11.11	8.41	51.53	39.95	11.11	8.36	51.29	39.84	11.04	8.36	10^{-2}
10.000	20.11	20.11	4.97	3.77	26.19	20.13	4.97	3.77	26.19	20.11	4.97	3.77	10^{-2}
12.589	10.08	10.08	2.21	1.69	13.30	10.08	2.21	1.68	13.29	10.09	2.21	1.68	10^{-2}
15.849	50.47	50.47	9.76	7.51	67.36	50.47	9.76	7.49	67.31	50.42	9.76	7.51	10^{-3}
19.953	25.22	25.22	4.31	3.33	34.03	25.29	4.33	3.33	34.03	25.26	4.31	3.36	10^{-3}
25.119	12.61	12.61	1.91	1.50	17.16	12.62	1.91	1.50	17.13	12.60	1.91	1.49	10^{-3}
31.623	63.51	63.51	8.59	6.78	87.22	63.48	8.56	6.75	87.23	63.52	8.58	6.73	10^{-4}

TABLE XX. Neutrino flux ($m^{-2}\,sec^{-1}\,sr^{-1}\,GeV^{-1}$) for $-0.9 \geq \cos\theta_z \geq -1.0$.

	Kamioka				Sudbury				Gran Sasso				
E_ν (GeV)	ν_μ	$\bar{\nu}_\mu$	ν_e	$\bar{\nu}_e$	ν_μ	$\bar{\nu}_\mu$	ν_e	$\bar{\nu}_e$	ν_μ	$\bar{\nu}_\mu$	ν_e	$\bar{\nu}_e$	Norm
0.1000	6.78	6.78	3.30	3.15	8.39	8.47	4.17	3.84	7.42	7.49	3.67	3.44	10^3
0.1259	5.51	5.51	2.66	2.51	6.76	6.80	3.34	3.03	6.02	6.04	2.96	2.72	10^3
0.1585	4.30	4.30	2.06	1.91	5.22	5.22	2.55	2.27	4.67	4.67	2.27	2.05	10^3
0.1995	3.18	3.18	1.53	1.39	3.81	3.79	1.86	1.63	3.44	3.42	1.67	1.48	10^3
0.2512	22.38	22.38	10.84	9.68	26.28	26.09	12.91	11.13	23.92	23.74	11.68	10.19	10^2
0.3162	15.05	15.05	7.34	6.44	17.32	17.13	8.55	7.25	15.93	15.75	7.78	6.72	10^2
0.3981	9.74	9.74	4.75	4.11	10.98	10.82	5.40	4.52	10.24	10.06	4.96	4.23	10^2
0.5012	6.07	6.07	2.95	2.52	6.73	6.57	3.28	2.71	6.36	6.20	3.04	2.56	10^2
0.6310	3.65	3.65	1.77	1.49	4.02	3.87	1.91	1.57	3.84	3.69	1.81	1.50	10^2
0.7943	21.51	21.51	10.22	8.50	23.48	22.26	10.84	8.82	22.63	21.52	10.31	8.52	10^1
1.0000	12.36	12.36	5.77	4.73	13.49	12.59	5.97	4.82	13.16	12.29	5.75	4.70	10^1
1.2589	6.95	6.95	3.15	2.55	7.67	7.01	3.21	2.57	7.54	6.89	3.13	2.53	10^1
1.5849	3.84	3.84	1.68	1.34	4.29	3.84	1.69	1.34	4.26	3.79	1.66	1.33	10^1
1.9953	20.67	20.67	8.67	6.86	23.70	20.66	8.68	6.83	23.55	20.51	8.60	6.79	10^0
2.5119	10.95	10.95	4.40	3.41	12.80	10.91	4.36	3.39	12.80	10.90	4.33	3.39	10^0
3.1623	5.71	5.71	2.14	1.65	6.85	5.68	2.13	1.64	6.84	5.68	2.13	1.64	10^0
3.9811	29.41	29.41	10.21	7.80	36.14	29.39	10.18	7.79	36.20	29.35	10.17	7.79	10^{-1}
5.0119	15.04	15.04	4.77	3.63	18.84	15.03	4.75	3.62	18.85	15.03	4.75	3.64	10^{-1}
6.3096	7.63	7.63	2.19	1.67	9.77	7.65	2.18	1.66	9.79	7.65	2.20	1.66	10^{-1}
7.9433	38.59	38.59	9.91	7.52	50.21	38.57	9.84	7.56	50.19	38.73	9.90	7.52	10^{-2}
10.000	19.33	19.33	4.43	3.36	25.51	19.36	4.43	3.37	25.50	19.35	4.43	3.37	10^{-2}
12.589	9.70	9.70	1.97	1.50	12.94	9.70	1.97	1.50	12.92	9.71	1.97	1.50	10^{-2}
15.849	48.53	48.53	8.66	6.70	65.52	48.58	8.70	6.71	65.41	48.57	8.70	6.71	10^{-3}
19.953	24.28	24.28	3.84	2.99	33.06	24.31	3.85	2.99	32.98	24.26	3.84	2.97	10^{-3}
25.119	12.08	12.08	1.70	1.34	16.61	12.10	1.69	1.34	16.60	12.10	1.70	1.33	10^{-3}
31.623	60.78	60.78	7.67	6.06	84.31	60.81	7.66	6.08	84.26	60.81	7.66	6.06	10^{-4}

[1] M. Honda, T. Kajita, K. Kasahara, S. Midorikawa, and T. Sanuki, Phys. Rev. D **75**, 043006 (2007).
[2] M. Honda, T. Kajita, K. Kasahara, and S. Midorikawa, Phys. Rev. D **70**, 043008 (2004).
[3] S. Roesler, R. Engel, and J. Ranft, arXiv:hep-ph/0012252.
[4] T. Sanuki, M. Honda, T. Kajita, K. Kasahara, and S. Midorikawa, Phys. Rev. D **75**, 043005 (2007).
[5] K. Hänssget and J. Ranft, Comput. Phys. Commun. **43** (1986).
[6] K. Niita *et al.*, Radiation Measurements **41**, 1080 (2006).
[7] H. Collaboration, Astropart. Phys. **29**, 257 (2008).
[8] H. Collaboration, Astropart. Phys. **30**, 124 (2008).
[9] T. K. Gaisser, Astropart. Phys. **16**, 285 (2002).
[10] S. Haino *et al.* (BESS), Phys. Lett. B **594**, 35 (2004).
[11] T. Sanuki *et al.*, Phys. Lett. B **541**, 234 (2002), see also erratum [24].
[12] K. Abe *et al.* (BESS), Phys. Lett. B **564**, 8 (2003).
[13] J. Alcaraz *et al.* (AMS), Phys. Lett. B **490**, 27 (2000).
[14] J. Alcaraz *et al.* (AMS), Phys. Lett. B **494**, 193 (2000).
[15] T. Sanuki *et al.* (BESS), Astrophys. J. **545**, 1135 (2000).
[16] T. K. Gaisser *et al.*, in *Proceedings of the 27th International Cosmic Ray Conference, Hamburg* [5, 1643 (2001)].
[17] T. K. Gaisser and M. Honda, Annu. Rev. Nucl. Part. Sci. **52**, 153 (2002).
[18] See http://nssdc.gsfc.nasa.gov/space/model/atmos/us_standard.html.
[19] See http://www.ngdc.noaa.gov/IAGA/vmod/igrf.html.
[20] G. D. Barr, T. K. Gaisser, P. Lipari, S. Robbins, and T. Stanev, Phys. Rev. D **70**, 023006 (2004).
[21] http://www-pnp.physics.ox.ac.uk/barr/fluxfiles/index.html.
[22] G. Battistoni, A. Ferrari, T. Montaruli, and P. R. Sala, Astropart. Phys. **19**, 269 (2003).
[23] P. Lipari, Astropart. Phys. **14**, 171 (2000).
[24] T. Sanuki *et al.*, Phys. Lett. B **581**, 272 (2004).